Wiley
International Journal of Energy Research
Volume 2024, Article ID 8811265, 22 pages
https://doi.org/10.1155/2024/8811265

WILEY

Research Article

Neutronic Analysis of Accident-Tolerant Cladding Materials in 3D Full Core BEAVRS PWR Benchmark Using OpenMC Code

Khalid A. Alamri,[1,2,3] **Meshari M. Alqahtani**,[4] **Abdullah S. Alomari**,[1,4] **and Abdullah I. Almarshad**[1]

[1]*MS in Nuclear Engineering Program, College of Engineering, King Saud University, Riyadh 12372, Saudi Arabia*
[2]*K.A.CARE Energy Research and Innovation Center, King Saud University, Riyadh 11421, Saudi Arabia*
[3]*Engineering and Project Management Sector, King Abdullah City for Renewable and Atomic Energy (K.A.CARE), Riyadh 11451, Saudi Arabia*
[4]*Nuclear Technologies Institute, King Abdulaziz City for Science and Technology (KACST), Riyadh 11442, Saudi Arabia*

Correspondence should be addressed to Khalid A. Alamri; 442105850@student.ksu.edu.sa

Received 22 August 2023; Revised 28 March 2024; Accepted 22 April 2024; Published 28 May 2024

Academic Editor: Andrey Kuzmin

After the Fukushima Daiichi nuclear accident in 2011, the performance of nuclear fuel during accidents became a matter of great concern. To address this, a new type of fuel technology called accident-tolerant fuel (ATF) has been developed with the goal of enhancing the ability of light water reactors (LWRs) to withstand severe accident conditions. Iron-based alloys have been suggested as potential candidates for fuel cladding due to their favourable thermomechanical properties, lower reactivity with steam, and lower hydrogen generation. This study evaluates the neutronic performance of C26M (a 2nd generation nuclear grade FeCrAl alloy), APMT™, 310SS, and 304SS cladding materials by comparing them with Zircaloy-4 cladding in a 3D PWR core at the beginning of the cycle (BOC) using OpenMC code. The results revealed that the neutronic penalty varied for different alternative cladding materials where C26M exhibited the lowest neutronic penalty value of -12551 pcm, while 310SS demonstrated the highest with a value of -17855 pcm. Additionally, important parameters in the reactor core such as neutron spectrum, reactivity coefficients, boron worth, control rod bank worth, power distribution, and radial thermal neutron flux distribution are evaluated and discussed. The analysis results showed that C26M provided a significantly higher level of neutronic performance compared to APMT™, 304SS, and 310SS. Although this study primarily focused on the neutronic performance of PWRs at BOC, future research should encompass fuel depletion analysis to delve deeper into the potential of alternative cladding materials.

1. Introduction

Light water reactors (LWRs) are the most commonly used nuclear reactors worldwide for the production of electricity [1]. The heat generated by the nuclear fuel in LWRs is transferred to the water, surrounding the fuel cladding tubes, resulting in the production of steam that drives turbines for electricity generation. Therefore, the fuel cladding serves as the main physical radiation protection barrier, effectively preventing the release of radioactive materials from the nuclear fuel into the water coolant. Choosing fuel cladding materials must satisfy various design constraints, such as low neutron absorption cross-section, reliable mechanical properties at elevated temperatures and in high radiation fields, sufficient thermal conductivity, and strong resistance to corrosion when exposed to water.

For decades, the cladding materials used in LWRs are typically made of zirconium-based alloys due to their outstanding performance, reliability, and extensive industrial experience. The popularity of these alloys can be attributed to their favourable characteristics, such as reasonable corrosion resistance, relatively low neutron absorption cross-section, good thermomechanical properties, and metallurgical manufacturability [2–5]. The predominant material in the

zirconium cladding is primarily zirconium, with a composition typically falling within the range of 97% to 99%. In addition, small amounts of other elements such as Sn, Fe, Cr, Nb, and Ni are incorporated to fine-tune and optimize the specific desired characteristics. These elements improve the alloy's performance by enhancing properties like deformation under stress (creep), expansion, corrosive effects, and absorption of hydrogen. However, zirconium-based alloys have limitations, particularly under severe accident scenarios [2–5]. Under normal operating conditions of nuclear reactors, zirconium-based alloys undergo a natural corrosion process that results in the formation of zirconium dioxide (ZrO_2) on the metal surface. However, this corrosion process accelerates when the alloy is exposed to high-temperature steam, such as during a loss-of-coolant accident (LOCA). The excess absorption of hydrogen beyond the solubility limit may lead to the formation of hydrides, which is the primary cause of ductility loss [2–5]. If the temperature reaches around 800°C, the cladding made of zirconium alloy will expand and rupture, which can release fission products into the primary coolant circuit. The exothermic reaction between zirconium and steam can also significantly accelerate when the temperature rises to about 1200°C, leading to the release of a significant amount of combustible hydrogen gas. These hydrogen gasses were responsible for the explosions that caused damage to the reactor buildings at the Fukushima Daiichi plant and contributed to the dispersion of radioactive substances into the environment [6, 7]. Thus, susceptibility to corrosion and hydrogen embrittlement are the main limitations for Zr-based alloys that are historically used as cladding materials.

In the aftermath of the Fukushima disaster in 2011, there has been a pressing need for research and development (R&D) of light water reactor (LWR) fuels to develop a new fuel system (fuel, cladding, and related systems) that improves fuel safety and reliability under accident conditions. This has led to the development of accident-tolerant fuels (ATFs), which are defined as fuels that can tolerate a longer period of loss of active cooling in the core than the current fuel-cladding (UO_2-Zircaloy) system, while maintaining or improving fuel performance during normal operations and operational transients [8]. There are three suggested approaches to enhance accident tolerance in the fuel and cladding of nuclear reactors [9]:

(1) Replacement or improvement of the current UO_2 ceramic fuel

(2) Modifications to the current zircaloy cladding for improved oxidation resistance, including coating layer design

(3) Replacement of the current zircaloy cladding with alternative cladding materials that have high oxidation-resistant properties

The development of alternative cladding materials for LWRs has been a topic of interest in recent years. In addition to the mechanical and metallurgical integrity constraints, alternative cladding materials need also to satisfy the neutronic design requirements such as criticality conditions, desired power distribution and profiles, and reactivity performance. Various studies have been conducted by researchers to analyse the neutronic performance of the alternate cladding materials in LWRs [10–13]. George et al. [10] have analysed the reactivity for alternative cladding materials by changing the cladding thickness, pellet diameter, and amount of enriched uranium to improve the reactivity and cycle length of the fuel. Also, the study showed results on the isotopic and total plutonium inventory during fuel lifetime for alternative cladding materials. Additionally, the study compares spectral hardening between alternative cladding designs and a reference Zircaloy-4 cladding case. This study used SCALE 6.1 code with ENDF/B-VII.0 library to model 2D Standard PWR fuel assembly (17×17). The alternate cladding materials examined in this study were FeCrAl, SS-310, SS-304, and APMT™. The study shows that replacing zirconium with iron-based alloy cladding in PWR fuel pins leads to a neutronic penalty, especially for austenitic stainless steels with nickel. Additionally, core reactivity can be improved for ferritic alloys by reducing cladding thickness or increasing enrichment by approximately 1%, whereas austenitic alloys may need higher enrichment, around 1.5%. Moreover, employing alternate cladding with higher thermal neutron capture cross-section slightly enhances plutonium breeding through spectrum hardening.

In another study by George et al. [11], parameter combinations of enrichment and cladding thickness have been determined to match the pressurized water reactor lifetime for alternative cladding materials (FeCrAl, SS-310, and SiC). They calculated reactivity coefficient, radial fission power, plutonium breeding, and fuel pellet costs for each design using SCALE 6.1 code with ENDF/B-VII.0 library to model 2D Standard PWR fuel assembly (17×17). The study demonstrates that using a thinner cladding (350 μm) allows austenitic stainless steels to require only a slight increase (0.5 wt %) in enriched ^{235}U, while FeCrAl requires a smaller increase (0.1%) to meet the specifications of the fuel cycle. The analysis also shows closely similar reactivity behaviours for coolant temperature and void perturbations in each cladding material, with FeCrAl and 310SS cladding leading to slightly elevated fission power near the pellet's periphery, thereby leading to an increased production of ^{239}Pu. The economic evaluation demonstrates that the adoption of FeCrAl alloys leads to a 15% rise in the production expenses of fuel pellets, primarily attributed to the need for higher enrichment and the utilization of thinner cladding.

Naceur and Marleau [12] evaluated the neutronic performance of different materials including SS-304, SS-310, FeCrAl, APMT™, and SiC in comparison to zirconium alloy. They employed several calculations such as burnup, isotope depletion, absorption rate ratios, spectral and spatial self-shielding analyses, plutonium radial profile, and reactivity perturbations. They utilized the DRAGON5 code to model a typical CANDU-6 lattice. The study indicates a neutronic penalty in iron and steel-based bundles caused by the significant thermal capture of nickel-59 and iron-56. To achieve CANDU-6 burnup average criticality, ferritic and steel-based claddings necessitate minimum enrichments of 1.0% and 1.1%, respectively. Furthermore, reducing the cladding thickness by 200 μm allows meeting criticality requirements

for all claddings with enrichments below 1%. SiC and Zr bundles exhibit higher moderator and coolant temperature coefficients, while FeCrAl, APMT™, 304SS, and 310SS claddings display elevated Doppler and voiding effects during mid-burnup.

Recently, Alhattawi et al. [13] investigated FeCrAl and SiC cladding materials in the APR-1400 reactor. They carried out a parametric evaluation of both fuel and cladding materials to determine the geometry requirements necessary for achieving the desired fuel reactivity at the end of the cycle. They then compared their results with the standard APR-1400 reference fuel-cladding system. The authors evaluated various parameters, including fuel reactivity, thermal neutron spectrum, plutonium inventory evolution, and pin power distribution when different cladding materials were utilized. They used a 2D model of a standard APR-1400 reactor fuel assembly to carry out this study. The study indicates that the elevated absorption cross-section values in FeCrAl cladding led to a decrease in K_{eff} values over the cycle, but an increase in fuel enrichment can effectively mitigate the neutronic penalty.

The studies cited above, and others, have evaluated alternative cladding materials focusing mainly on fuel pin and assembly models to assess the performance of alternative cladding materials in LWRs. However, these models were mostly simplified in 2D models. Detailed designs are imperative to validate these preliminary studies. Moreover, beyond fuel and cladding materials, other core components, such as control rods, must be considered to evaluate alternative cladding materials for safety and to ensure accurate neutronic calculations. In addition, prior studies did not account for alternative materials in grid spacers. Accurate neutronic calculations are vital for reactor safety [14]. The spacer grid in fuel assemblies provides essential support to fuel rods [14]. Its inclusion in modelling is crucial to evaluate alternative cladding materials, which impacts neutronic performance and aids in selecting materials for improved reactor safety and efficiency. Furthermore, previous studies on the evaluation of the performance of alternative cladding materials utilized various tools such as Serpent, SCALE 6.1, and MCNPX codes and various benchmarks like APR-1400, VERA, and AP1000. They focused on different and separate aspects in the study of alternative materials, such as neutronic penalties, design modifications, the worth of control rods, and boron concentration. Furthermore, previous studies did not cover the recently developed and optimized alloy of FeCrAl with improved mechanical properties, resulting in limited studies of the neutronic performance of such new alloys.

In this study, we utilized the BEAVRS benchmark to evaluate alternative cladding materials, employing the OpenMC code for modelling and analysing neutrons in the assessment of alternative cladding materials. Both the BEAVRS benchmark and the OpenMC code are open source, enhancing the accessibility and extendibility of our study. This contribution is vital to the overall importance of the topic by facilitating further exploration and collaboration in the scientific community. Furthermore, the diversity in using benchmarks and codes in evaluating alternative cladding materials offers more comprehensive insights, enhancing the output extracted from various research studies. Neutron calculations will be conducted to investigate how alternative cladding materials including newly developed materials behave in a 3D full PWR core at the beginning of the cycle (BOC). First, the reactivity penalty of alternative cladding materials will be calculated in cases where only the cladding material or both the cladding and grid spacers are substituted with alternative materials. Second, a parametric study of both fuel and cladding materials will be performed to overcome the reactivity penalty of alternative cladding materials and match the performance of Zircaloy-4 cladding. Third, the study will assess the impact of changing the material and the modified fuel rods on different parameters, including the neutron spectrum, reactivity coefficients, boron worth, control rod bank worth, power distribution, and thermal neutron flux distribution, when using different cladding materials.

2. Methodology

2.1. Austenitic Steels and Ferritic Alloys. In this study, two types of iron-based alloys were investigated, namely, two austenitic stainless steels (hereafter refer as 310SS and 304SS) and two ferritic alloys (hereafter refer as C26M alloy and commercial APMT™ alloy (FeCrAlMo)). Table 1 shows the chemical compositions for the C26M (Fe-12Cr-6Al-2Mo-0.2Si-0.03Y), APMT™, 310SS, and 304SS cladding materials employed in this study.

Type 304SS was chosen as a case study due to its historical use as a cladding material in the early decades of nuclear reactors [15], even though it does not offer exceptional oxidation resistance at high temperatures [16]. Type 310SS, on the other hand, has higher chromium and nickel contents, which makes it more resistant to high-temperature steam oxidation by forming a protective Cr_2O_3 scale [17]. Ferritic alloys were selected as the cladding material under investigation due to their excellent high-temperature steam oxidation, corrosion performance, and high-temperature strength [18]. With a significant aluminium content, ferritic alloys generate a protective Al_2O_3 layer during high-temperature oxidation that possesses greater strength than the layer formed in austenitic steels [17, 19]. Similar to Cr_2O_3, Al_2O_3 has lower permeability compared to ZrO_2, resulting in significantly enhanced oxidation properties, especially in the presence of high-temperature steam [19]. This study is involving also the recently developed and optimized alloy of FeCrAl C26M, which is a 2nd generation FeCrAl alloy with a nominal composition of Fe-12Cr-6Al-2Mo-0.2Si-0.03Y with improved mechanical properties and limited studies of neutronic performance of such new alloy [20].

The primary drawback of iron-based alloys is their neutron absorption cross-section, which is significantly higher (about fifteen times) than that of zirconium alloys, as shown in Figure 1. This results in a fuel enrichment penalty. Table 2 presents the cladding materials examined in this study along with their density and macroscopic thermal neutron absorption cross-section ($\sum_{\text{abs}}^{\text{therm}}$) taken at a neutron energy of 0.025 eV.

Iron-based alloys have higher strength than zirconium alloys and are less susceptible to cladding thickness loss

Table 1: Alternative cladding material compositions.

wt %	Cladding material				
	Zircaloy-4	C26M	APMT™	304SS	310SS
Fe	0.21	79.42	69.79	71.35	52.5
Cr	0.1	12.2	21.6	18.9	25.2
Al		6.1	4.9		
Zr	98.115		0.1		
Ni				8.35	19.5
Sn	1.45				
Mn				0.7	1.9
Mo		2.04	2.8	0.27	0.13
Y		0.04	0.12		
Si		0.2	0.53	0.42	0.7
Hf			0.16		
O	0.125				
Ref.	[21]	[20]		[10]	

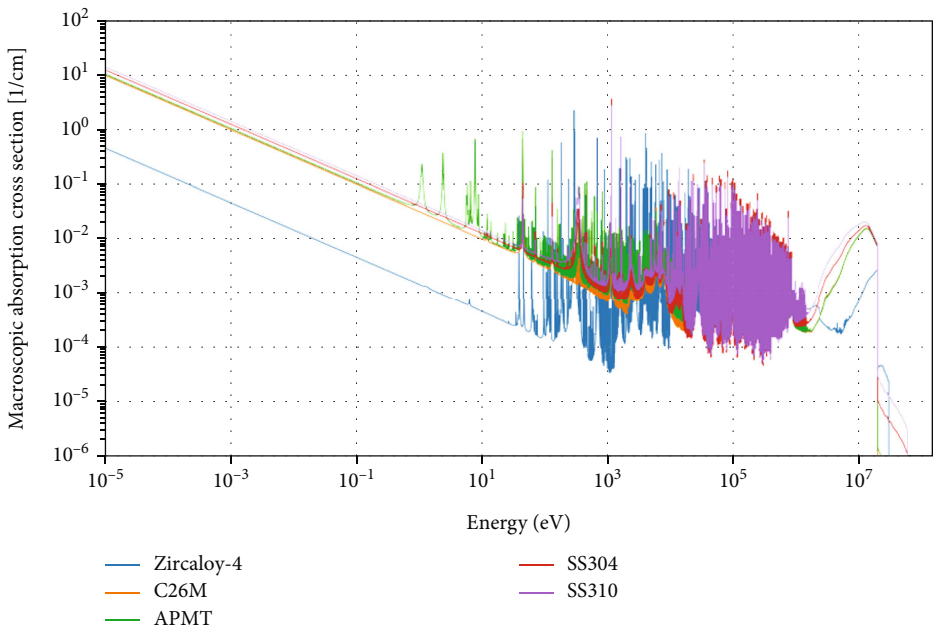

Figure 1: Macroscopic neutron absorption cross-sections for several cladding material options by OpenMC.

Table 2: Alternative cladding density and average thermal absorption cross-section.

Material	Density (g/cm^3)	$\sum_{abs}^{therm}$ (cm^{-1})[a]	Ref.
Zircaloy-4	6.55	0.00903	[21]
C26M	7.2	0.19549	[22]
APMT™	7.3	0.20936	
304SS	7.9	0.24723	[10]
310SS	8.03	0.27957	

[a]Macroscopic thermal neutron absorption cross-section by OpenMC.

due to corrosion under normal operating conditions, allowing for a reduction in cladding thickness and an increase in pellet size (assuming a constant pitch-to-diameter ratio (P/D)) [11].

Previous studies on iron-based cladding [15] indicated that achieving comparable fuel cycle lengths to zirconium alloy-clad fuel assemblies in LWRs involved implementing strategies such as decreasing cladding thickness, enhancing fuel enrichment, and elevating fuel stack heights.

2.2. BEAVRS Benchmark Description. The BEAVRS benchmark provides an extensive set of information needed to construct the neutronic calculation model of a commercial pressurized water reactor (PWR) core [21]. This information includes detailed geometry and material specifications for the pin cell types, fuel assembly design, and core, with both the radial and axial geometry [23]. For pin cells, the specifications include fuel pins, burnable poisons, guide tubes, and instrument tubes. Furthermore, the benchmark provides

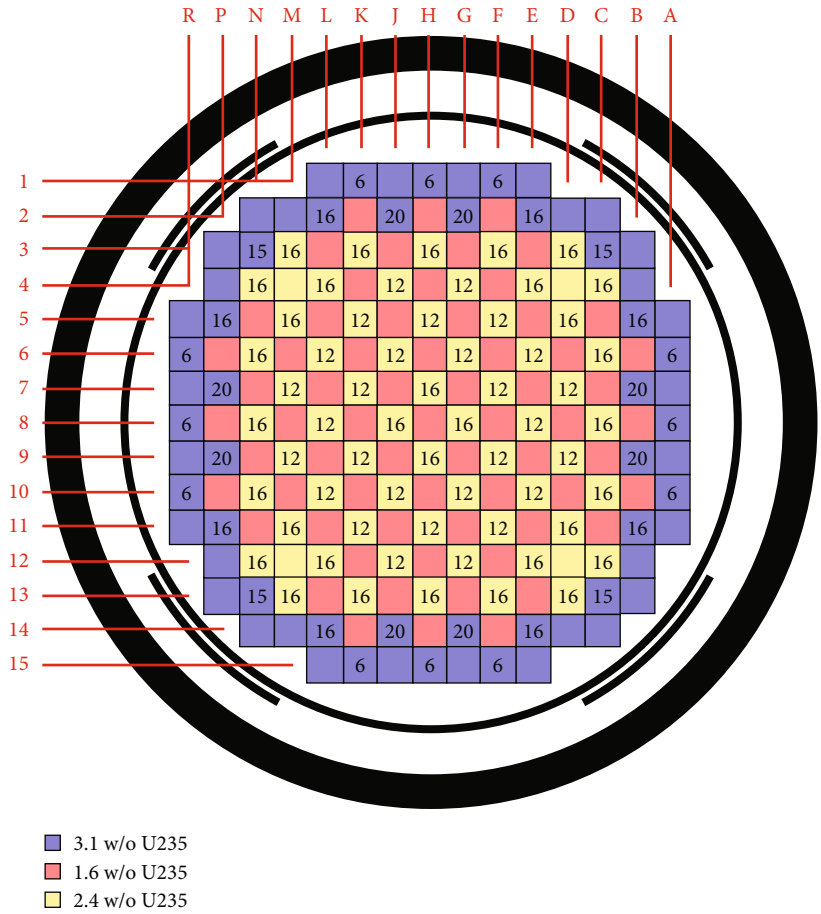

Figure 2: Enrichment loading pattern and number and positions of the burnable absorber in cycle 1 [21].

information on the upper and lower structures of the reactor, encompassing various aspects such as plenum regions, end plugs, upper and lower nozzles, and support plates [23]. Fuel assembly specifications cover the locations of burnable absorbers within guide tubes and grid spacers [23]. The core loading pattern includes assemblies with different fuel enrichment, burnable poison rods, incore instruments, and control rod bank. The benchmark also includes information on in-vessel structures like the baffle plate, core barrel, four neutron shield panels, the reactor pressure vessel, and liner [21]. Figures 2 and 3 depict the core arrangement presentation, providing an overview of various key elements as obtained from the BEAVRS benchmark [21]. These include the enrichment of U-235, the distribution of burnable absorbers, control rod banks, and shutdown banks in terms of their number and specific locations within the core, as well as the positioning of instrument tubes.

The main specifications of the BEAVRS benchmark are provided in Table 3; for a detailed description of the BEAVRS benchmark, the reader may refer to [21]. The benchmark also includes data on operational conditions and measurement results for validation, such as in-core detector signals and reactor physics test results for cycles 1 and 2.

The BEAVRS benchmark is an important tool for improving the accuracy and reliability of the neutronic calculation of PWRs. By providing a standardized framework for evaluating and comparing different codes and models, it enables researchers and developers to identify areas where improvements can be made. This can lead to more accurate and reliable neutronic calculation, which can in turn enhance the safety and efficiency of PWRs.

2.3. OpenMC 3D Core Model. OpenMC is a code designed for Monte Carlo neutron and photon transport simulation. It has the ability to conduct fixed source, k-eigenvalue, and subcritical multiplication calculations on models that are built utilizing either constructive solid geometry or CAD representation [24]. OpenMC has the capacity to handle both continuous-energy and multigroup transport. The particle interaction data in a continuous-energy format is derived from a native HDF5 structure, which has the capability to be generated from the ACE format employed in the MCNP and Serpent code. Parallelism is made possible through a hybrid MPI and OpenMP programming model. OpenMC code has been created by the Computational Reactor Physics Group (CRPG) members at the MIT in 2011. But it is now being developed by a diverse group of universities, laboratories, and other organizations [24]. The OpenMC is an open-source code that can perform high-performance and precise calculations for k-eigenvalue, burnup rate, fission rate, and flux distribution, [25]. The code can be written using either Python or the C/C++ language.

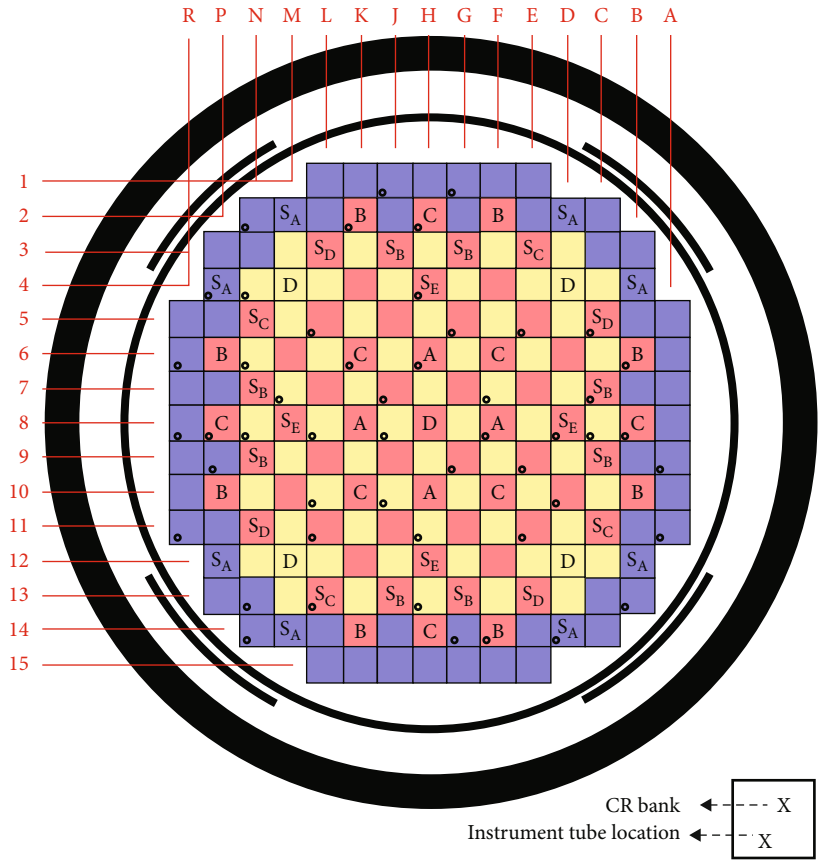

Figure 3: CR banks and instrument tube locations [21].

A detailed 3D core of the benchmark design was modelled using the OpenMC Code and the Evaluated Neutron Data File library, ENDF/B-VII.1 [26]. The model was prepared to include all the details provided in the BEAVRS benchmark [21]. Initially, the fuel rods, guide tubes, instrument tubes, burnable absorbers, and control rods were modelled with different axial zones. Then, these models were used to create fuel assemblies in a 17×17 array of pins for the initial core, according to fuel enrichment, presence of burnable absorbers, guide tubes, and instrument tube. Additionally, each fuel assembly model had eight grid spacers, with the middle six consisting entirely of Zircaloy-4 and the top and bottom spacers consisting of a Stainless Steel 304 (SS304) sleeve with Inconel internal structures.

Finally, the fuel assembly models were used to create the 3D BEAVRS core model, which includes 193 fuel assemblies loaded in a 15×15 array according to the loading pattern. In addition to the fuel assemblies, the 3D model also includes the baffle, barrel, neutron shielding panel, and vessel. The baffle is a structure that surrounds the core to direct the flow of coolant, while the barrel is a cylindrical structure that supports the fuel assemblies. The neutron shielding panel is a layer of material that absorbs neutrons to prevent them from escaping the core, and the vessel is a container that holds the coolant and provides structural support for the core. The detailed modelling of these components allows for a more accurate simulation of the behaviour of the core under different conditions.

In order to achieve precise and accurate results from the OpenMC code, it is important to evaluate the convergence of the fission source distribution. This convergence is evaluated by utilizing the Shannon entropy, as defined in Equations (1) and (2) [27], to monitor the source distribution.

$$S_i = \frac{\text{Source sites in } i\text{th mesh element}}{\text{Total number of source sites}}, \tag{1}$$

$$H = -\sum_{i=1}^{N} S_i \log_2 S_i, \tag{2}$$

where S_i is the fraction of source sites that are present in each mesh element which is a structured mesh over the geometry that contains all fissionable materials. H is the Shannon entropy, i is the mesh element, and N is the number of mesh elements. If the source is well-distributed, there should be a consistent statistical constancy of the Shannon entropy throughout the generation cycle. This constancy can help identify the precise number of cycles that must be skipped. A useful approach to identify the skipping of cycles is to plot the Shannon entropy against the cycle number.

In this work, The OpenMC simulation runs were performed on a Windows computer (Intel Xeon E5-2670 @ 2.3 GHz) 48-core processors. A total of 400 million particles were used with 200 inactive cycles, 2000 active cycles, and

Table 3: The main specifications of the BEAVRS benchmark [21].

Core	
Thermal power	3411 MWth
Operating pressure	15.5 MPa
Fuel assembly	
Number of fuel assemblies	193
Fuel assembly design	17×17
Assembly pitch	21.50364 cm
Active fuel length	365.76 cm
Number of fuel rods	264
Fuel rod	
Pellet material	UO_2
^{235}U enrichment	1.6 wt % (fuel type 1), 2.4 wt % (fuel type 2), 3.1 wt % (fuel type 3)
Fuel density for 1.6/2.4/3.1 wt %	10.31341/10.29748/10.30166 g/cm^3
Pellet radius	0.39218 cm
Cladding material	Zircaloy-4
Cladding inner radius	0.40005 cm
Cladding outer radius	0.45720 cm
Rod pitch	1.25984 cm
Control	
Number of control rod banks	57
Control rod material (upper region)	B_4C
Control rod material (lower region)	Ag-In-Cd
Number of burnable poison rods in core	1266
Burnable absorber material	Borosilicate glass
Grid spacer	
Number of spacer grid	8
Top/bottom grid spacer material	Inconel 718
Top/bottom grid sleeve material	SS304
Intermediate grid spacer and sleeve material	Zircaloy-4
Structure material	
Baffle	SS304
Core barrel	SS304
Neutron shield	SS304
Pressure vessel liner	SS304
Pressure vessel	Carbon steel 508

200,000 particles. The generation of plots and data postprocessing was carried out using the Python programming language.

2.4. Study Procedure. The study encompassed four main steps to assess alternative cladding materials for their applicability in nuclear fuel rods. The procedure involved (1) validating the accuracy and reliability of the 3D core model, (2) quantifying the reactivity penalty associated with the use of alternative cladding materials, (3) conducting a comprehensive parametric study to optimize both fuel and cladding materials, aiming to overcome the reactivity penalty of alternative cladding materials and match the performance of Zircaloy-4 cladding, and (4) analysing the impact of different cladding materials and modified fuel rods on various crucial parameters, such as neutron spectrum, reactivity coefficients, boron worth, control rod bank worth, power distribution, and thermal neutron flux distribution. A visual representation of the study procedure is presented in Figure 4, and a detailed description for each step is given below.

2.4.1. Validation of 3D Reactor Core of BEAVRS Model. The first step of the study is the validation of the 3D core model using OpenMC by comparing the results with the measured values of the BEAVRS benchmark. The purpose of the first step is to ensure the validity of the 3D core model and the accuracy and reliability of neutronic calculation before beginning the alternative cladding material assessment. In the first step, the effective multiplication factor (K_{eff}) was calculated for various control bank insertions and corresponding boron concentrations at the HZP core during cycle 1, based on the benchmark for each problem as well as the control rod bank worth for D bank. Tables 4 and 5 provide problems used for testing criticality and control rod bank worth at BEAVRS cycle 1 HZP, respectively.

Equation (3) [28] is used to estimate the difference in reactivity ($\Delta\rho$) between calculated and reference values. Additionally, Equation (4) [29] is utilized to determine the worth of the rod bank. To calculate the control worth for the bank, all control rods in the bank are fully withdrawn and all control rods for the same bank are fully inserted.

$$\Delta\rho\,(\text{pcm}) = \left(\frac{1}{K_{\text{reference values}}} - \frac{1}{K_{\text{calculated values}}}\right) \times 10^5, \quad (3)$$

$$\rho(\text{pcm}) = \left(\frac{1}{k_{\text{out}}} - \frac{1}{k_{\text{in}}}\right) \times 10^5. \quad (4)$$

2.4.2. Neutronic Assessment for Alternative Cladding Materials. The reactivity was a parameter used to evaluate the neutronic performance for alternative cladding materials. The evaluation process involved comparing the performance of these alternative materials against Zircaloy-4 as the reference case. The evaluation was conducted using the 3D reactor core of the BEAVRS model. The study focused on assessing the performance of the cladding materials with the beginning of the cycle (fresh fuel) during normal operation, without addressing the issue of fuel depletion. All calculations were performed with a supercritical core.

The reference case is the specification of the BEAVRS benchmark, in which cladding thickness is 571.5 μm and enrichments are 1.6, 2.4, and 3.1 w/o U-235 for fuel types 1, 2, and 3, respectively. Throughout this study, the boron concentration is equal to 378 ppm as an average value during the first cycle for BEAVRS [30] and all control rods are fully withdrawn (ARO). The temperatures of the fuel, clad, and moderator were set as 900 K, 600 K, and 580 K, respectively.

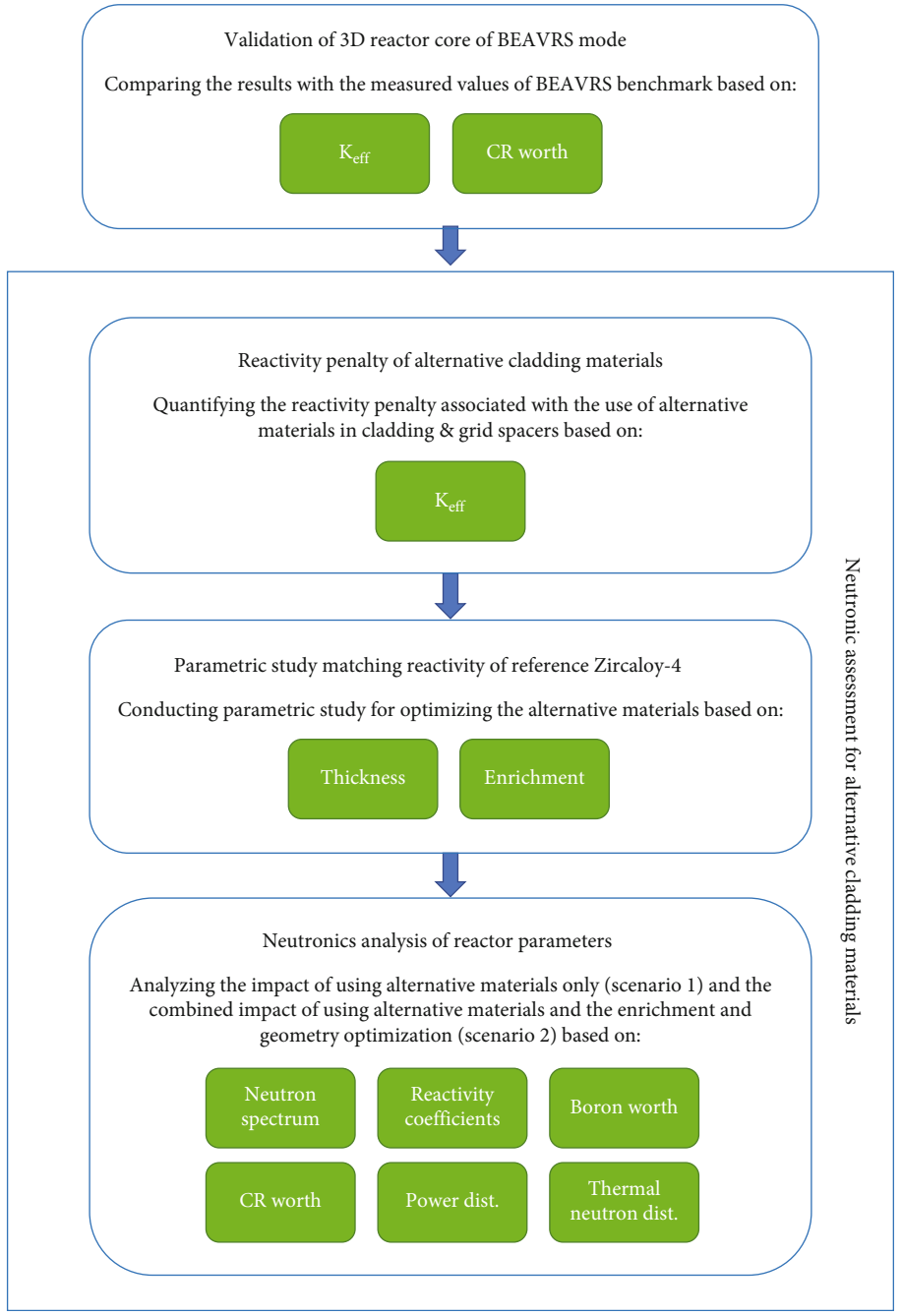

Figure 4: Flowchart of study procedure.

Table 4: Problems with different control rod statuses and boron concentration.

Problem	Configuration	Boron concentration (ppm)
A-1-1	ARO (all rods out)	975
A-1-2	D in	902
A-1-3	C, D in	810
A-1-4	B, A, D, C in	686
A-1-5	SD, SC, SE, D, C, B, A in	508

(1) Reactivity Penalty of Alternative Cladding Materials. Initially, the reactivity of alternative cladding materials was calculated to evaluate their performance in the reactor core for two cases. In the first case (B-1-1), only the cladding material was changed to alternative materials. In the second case (B-1-2), both the cladding and grid spacer materials were replaced with alternative materials. The purpose of these two cases was to analyse the effect of the change in reactivity of the core for the cladding alone and for the cladding with grid spacers.

Table 5: Control rod worth problem.

Problem	Rod	Inserted rod	Boron concentration (ppm)
A-2-1	D	ARO	902

Table 6: Case B-2: increase of U-235 enrichment level.

Problem	Increase of U-235 enrichment (%)	Fuel type 1	Fuel type 2	Fuel type 3
B-2-1	1.30%	2.28%	3.41%	4.40%
B-2-2	1.40%	2.34%	3.48%	4.50%
B-2-3	1.50%	2.39%	3.56%	4.60%
B-2-4	1.60%	2.44%	3.64%	4.70%
B-2-5	1.70%	2.49%	3.72%	4.80%
B-2-6	1.80%	2.54%	3.79%	4.90%
B-2-7	1.90%	2.60%	3.87%	5.00%
B-2-8	2.00%	2.65%	3.95%	5.10%
B-2-9	2.10%	2.70%	4.02%	5.20%
B-2-10	2.20%	2.75%	4.10%	5.30%

Table 7: Case B-3: decrease of cladding thickness.

Problem	Cladding thickness (μm)
B-3-1 (ref)	570.1
B-3-2	550
B-3-3	500
B-3-4	450
B-3-5	400
B-3-6	350
B-3-7	300
B-3-8	200
B-3-9	100

Table 8: Case B-4: combinations of decreased cladding thickness and increased enrichment level of U-235.

Problem	Increase of U-235 enrichment (%)	Fuel type 1	Fuel type 2	Fuel type 3
B-4-1	0.60%	1.92%	2.86%	3.70%
B-4-2	0.70%	1.97%	2.94%	3.80%
B-4-3	0.80%	2.03%	3.02%	3.90%
B-4-4	0.90%	2.08%	3.10%	4.00%
B-4-5	1.00%	2.13%	3.17%	4.10%
B-4-6	1.10%	2.18%	3.25%	4.20%
B-4-7	1.20%	2.23%	3.33%	4.30%
B-4-8	1.30%	2.28%	3.41%	4.40%

Equation (5) was used to estimate the difference in reactivity ($\Delta\rho$) between the alternative cladding materials and the Zircaloy-4 cladding, which represents the reactivity penalty of the alternative cladding materials.

Table 9: Boron concentrations.

Problem	Configuration	Boron concentration (ppm)
B-5-1	ARO	1000
B-5-2		500
B-5-3		378
B-5-4		0

Table 10: Different control rod statuses.

Problem	Configuration	Boron concentration (ppm)
B-6-1	ARO	
B-6-2	D in	378
B-6-4	All rod in	

$$\Delta\rho(\text{pcm}) = \left(\frac{1}{K_{\text{reference cladding}}} - \frac{1}{K_{\text{alternative cladding}}}\right) \times 10^5. \quad (5)$$

(2) Parametric Study Matching Reactivity of Reference Zircaloy-4. Next, multiple iterations of simulation were conducted to overcome the reactivity penalty of alternative cladding materials and match the performance of Zircaloy-4 cladding at the beginning of the cycle. Specifically, for each alternative cladding material, three cases of interest were examined in order to overcome the reactivity penalty. In each of these cases, both the cladding and grid spacer materials were replaced with alternative cladding materials.

The first case (B-2) maintained the thickness of alternative cladding materials as same in the reference case while increasing the enrichment level of U-235. To maintain the design basis parameters, the fuel type 3 is raised by 0.1 increment, and the enrichments of fuel types 1 and 2 are also increased with keeping the same ratio of enrichment between the three fuel types as in the reference case [31].

The second case (B-3) maintained the enrichments of fuel types 1, 2, and 3 as same in the reference case while decreasing the thickness of alternative cladding materials. This allows for increased heavy metal loading to overcome the reactivity penalty.

For the third case (B-4), the thickness of alternative cladding materials was set to a reasonably conservative value of 350 μm [32] while increasing the enrichment level of U-235 to identify combinations that overcame the reactivity penalty. Case 3 takes into consideration that it should not exceed the value of 5% of the enrichment level of U-235, referring to international practices for light water reactors (LWRs) [33] and reduced cladding thickness to 350 μm which is consistent with historic utilization of iron-based alloys as fuel cladding in LWRs [15, 19]. Also, it is considered that fuel type 3 is raised by 0.1 increment, and the enrichments of fuel types 1 and 2 are also increased with keeping the same ratio of enrichment between the three fuel types as in the reference case [31]. The outer rod diameter of

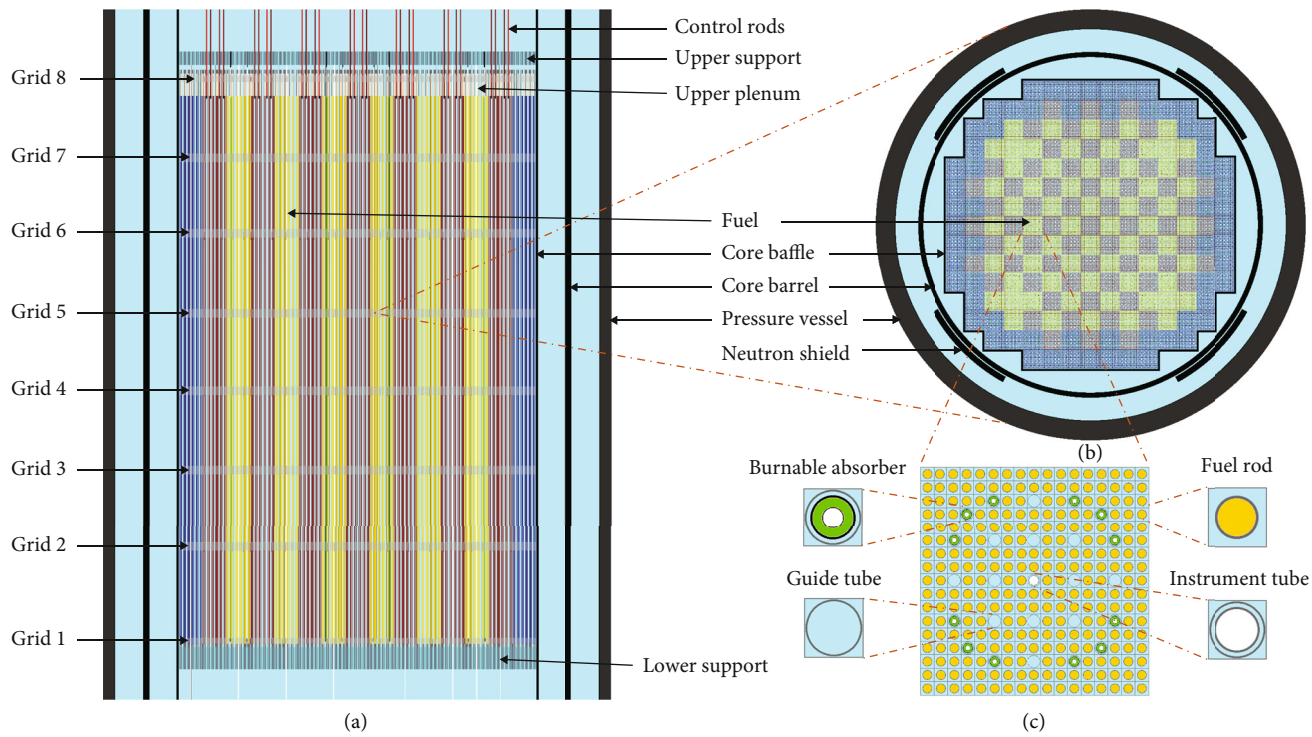

Figure 5: (a) Scale view of row 8 core axial cross-section, with highlighted grid simulated by OpenMC. (b) Scale view of grid 5 center core radial cross-section displaying radial structures and enrichment loading pattern. In this view, stainless steel is represented in black, carbon steel in dark gray, borated water in light blue, and the regions with 1.6, 2.4, and 3.1 w/o U235 are depicted in red, yellow, and dark blue, respectively. (c) Scale view of grid 5 center assembly-L8 radial cross-section indicating fuel rods, guide tubes, instrument tube, and burnable absorbers. Gray denotes zircaloy, green denotes burnable absorber, and white denotes air.

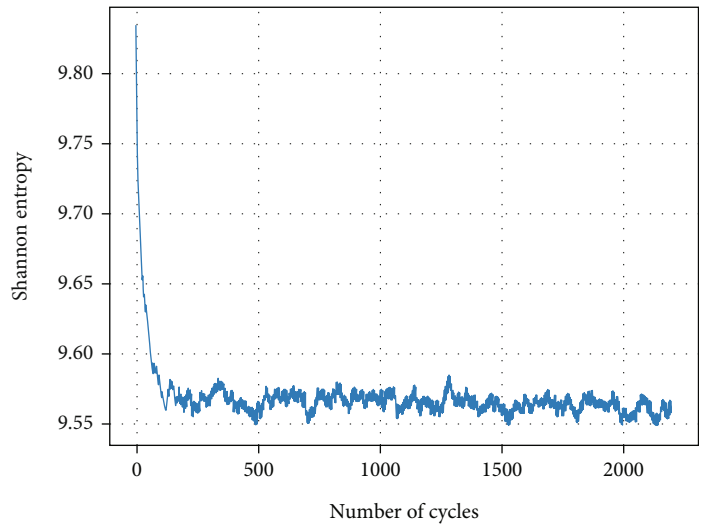

Figure 6: Shannon entropy against the cycle number.

0.9144 cm was fixed in all cases to maintain a fuel rod pitch-to-diameter ratio (P/D) of 1.37. This was done to ensure that the thermal hydraulics of the PWR system would not undergo significant changes upon commercialization [19]. Also, a pellet-cladding gap of 0.00787 cm is fixed in all cases [19]. Tables 6–8 present the problems for case B-2, case B-3, and case B-4, respectively.

(3) Neutronic Analysis of Reactor Parameters. After the parametric study was conducted, the effects of utilizing alternative cladding materials were evaluated on various factors, including the neutron spectrum, two reactivity coefficients (fuel temperature coefficient (FTC), moderator temperature coefficient (MTC)), boron worth, control rod bank worth, power distribution, and thermal neutron flux distribution.

Table 11: Results of K_{eff} for different control rod statuses and boron concentration.

Configuration	Boron concentration (ppm)	K_{eff}		$\Delta\rho$ (pcm)
		Measurement	OpenMC	
ARO (all rods out)	975	1.00000	1.00014 ± 0.00004	14
D	902	1.00000	1.00176 ± 0.00004	176
C, D	810	1.00000	1.00088 ± 0.00004	88
B, A, D, C	686	1.00000	0.99921 ± 0.00004	-79
SD, SC, SE, D, C, B, A	508	1.00000	0.99766 ± 0.00004	-235

Table 12: Control rod worth for D bank.

Configuration	Boron concentration (ppm)	K_{eff}		Measurement (pcm)	OpenMC (pcm)
		In	Out		
D in	902	1.00176 ± 0.00004	1.00958 ± 0.00004	788	773

Table 13: Case B-1-1: neutronic penalty for changing only the cladding material.

Problem	Material	K_{eff}	$\Delta\rho$-penalty (pcm)
B-1-1-A	Zircaloy-4	1.07248 ± 0.00004	—
B-1-1-B	C26M	0.95222 ± 0.00004	-11776
B-1-1-C	APMT™	0.93523 ± 0.00004	-13684
B-1-1-D	304SS	0.92590 ± 0.00004	-14761
B-1-1-E	310SS	0.90875 ± 0.00004	-16799

Table 14: Case B-1-2: reactivity penalty for changing the cladding and grid spacer material.

Problem	Material	K_{eff}	$\Delta\rho$-penalty (pcm)
B-1-2-A	Zircaloy-4	1.07248 ± 0.00004	—
B-1-2-B	C26M	0.94524 ± 0.00004	-12551
B-1-2-C	APMT™	0.92734 ± 0.00004	-14594
B-1-2-D	304SS	0.91787 ± 0.00004	-15706
B-1-2-E	310SS	0.90012 ± 0.00004	-17855

Table 15: The enrichment increase required to overcome the penalty observed at Case B-2 for alternative cladding materials.

Material	Fuel type 1	Fuel type 2	Fuel type 3
Zircaloy-4	1.61006%	2.39993%	3.10221%
C26M	2.37263%	3.53661%	4.57151%
APMT™	2.51952%	3.75556%	4.85453%
304SS	2.57770%	3.84228%	4.96663%
310SS	2.72390%	4.06021%	5.24832%

The effects of using alternative cladding materials were examined based on two scenarios. Scenario 1 examined the impact of using alternative cladding materials while keeping the enrichment and geometry of the fuel rods as specified in the reference case. Meanwhile, scenario 2 evaluated the combined impact of using alternative cladding materials and modifications to the enrichments and geometry of the fuel rods required to overcome the reactivity penalty and achieve performance comparable to Zircaloy-4.

The FTC is a measure of the change in reactivity per one Kelvin variation in fuel temperature. It is calculated according to the following equation [34]:

$$\frac{\Delta\rho}{\Delta T} = \frac{k_{\text{eff}}(T_2) - k_{\text{eff}}(T_1)}{k_{\text{eff}}(T_1) \times k_{\text{eff}}(T_2) \times (T_2 - T_1)} \times 10^5 \left[\frac{\text{pcm}}{k}\right], \quad (6)$$

where T_1 and T_2 are two fuel temperatures, while k_{eff} (T_1) and k_{eff} (T_2) are corresponding criticality values. The FTC is expressed in units of pcm per K. T_1 and T_2 were set to 900 K and 1000 K, respectively.

The MTC is a parameter that quantifies the impact of changes in reactor coolant temperature on reactivity. It is defined as the change in reactivity per one Kelvin change in moderator temperature. It is calculated using Equation (6), where T_1 and T_2 are two moderator temperature values, k_{eff} (T_1) and k_{eff} (T_2) are corresponding criticality values. The MTC is expressed in units of pcm per K. T_1 and T_2 were set to 580 K and 600 K, respectively. The densities of water at the given temperatures have been derived from Lemmon et al. [35]. The density of water at T_1 was found to be 0.7119 g/cm3, while at T_2, it was 0.66118 g/cm^3.

The boron worth (BW) is calculated as the change in reactivity per one ppm change in the soluble boron concentration, using the following equation [34]:

$$\frac{\Delta\rho}{\Delta BC} = \frac{k_{eff}(B_2) - k_{eff}(B_1)}{k_{eff}(B_1) \times k_{eff}(B_2) \times (B_2 - B_1)} \times 10^5 \left(\frac{\text{pcm}}{\text{ppm}}\right), \quad (7)$$

where B_1 and B_2, two boron concentrations, k_{eff} (B_1), and k_{eff} (B_2) are corresponding criticality values. Table 9 presents the varying concentration of boron in the moderator, ranging from 0 to 1000 ppm.

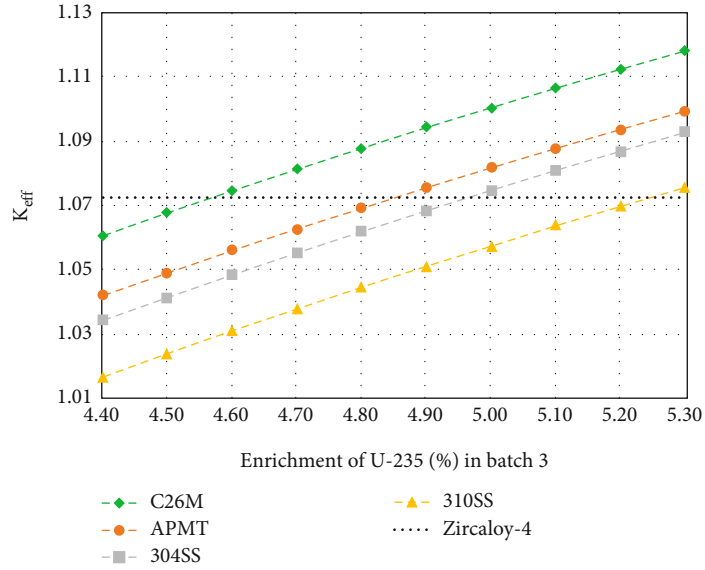

Figure 7: Case B-2: K_{eff} as a function of enrichment level in 571.5 μm of cladding thickness.

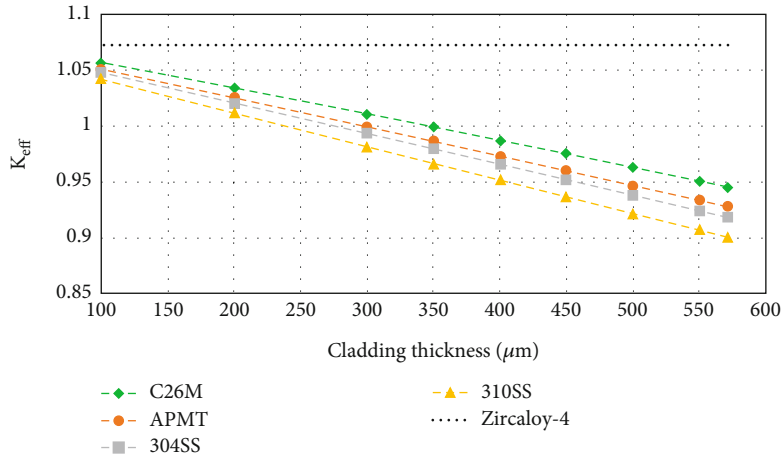

Figure 8: Case B-3: K_{eff} as a function of cladding thickness.

The control rod bank worth is calculated by considering the difference in criticality. It is computed using Equation (4), and Table 10 presents problems for different configuration banks.

3. Results and Discussion

3.1. Validation of 3D Reactor Core of BEAVRS Model. The 3D reactor core of the BEAVRS model was simulated using the OpenMC Code, along with the Evaluated Neutron Data File library ENDF/B-VII.1 [26]. The temperature values for the fuel, cladding, coolant, and structural materials were set at 566 K. Fuel enrichments were 1.6, 2.4, and 3.1 wt % with an exterior fuel pellet radius of 3.9218 mm, helium gap of 78.7 μm, and cladding thickness of 571.5 μm. It is important to note that this model was developed based on the hot zero power (HZP) condition for validation purposes. Any modifications made to the model for assessing alternative cladding materials are described in the methodology section.

The 3D BEAVRS core model generated by OpenMC is illustrated in Figure 5. To ensure the convergence of the neutron source, a source convergence test was conducted utilizing the Shannon entropy. Figure 6 indicates that excluding 200 cycles is necessary to obtain reliable results. The multiplication factor and control bank worth were calculated using OpenMC. These calculated values were then compared to the measured values obtained from the BEAVRS benchmark [21] to assess their accuracy and reliability.

3.1.1. Effective Multiplication Factor. The calculation of effective multiplication factors (K_{eff}) was carried out for various control bank insertions and corresponding boron concentrations at the HZP core during cycle 1, based on the benchmark for each case [21]. The K_{eff} values obtained are presented in Table 11, indicating that the BEAVRS model has demonstrated a satisfactory level of accuracy in

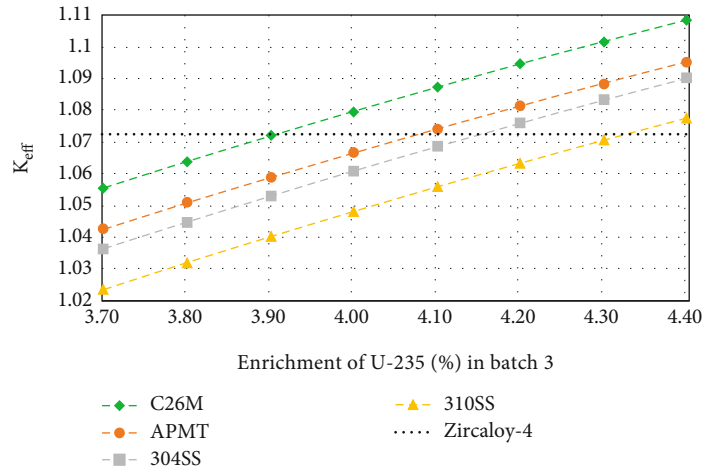

Figure 9: Case B-3: K_{eff} as a function of enrichment level in 350 μm of cladding thickness.

Table 16: The enrichment increase required to overcome the penalty observed at 350 μm for alternative cladding materials.

Material	Fuel type 1	Fuel type 2	Fuel type 3	Thickness (μm)	K_{eff}	$\Delta\rho$ (pcm)
Zircaloy-4	1.61006%	2.39993%	3.10221%	571.5	1.07248 ± 0.00004	—
C26M	2.02932%	3.02487%	3.91002%	350	1.07252 ± 0.00005	3
APMT™	2.11790%	3.15691%	4.08071%	350	1.07252 ± 0.00005	3
304SS	2.15702%	3.21521%	4.15607%	350	1.07255 ± 0.00005	6
310SS	2.24715%	3.34957%	4.32974%	350	1.07256 ± 0.00005	7

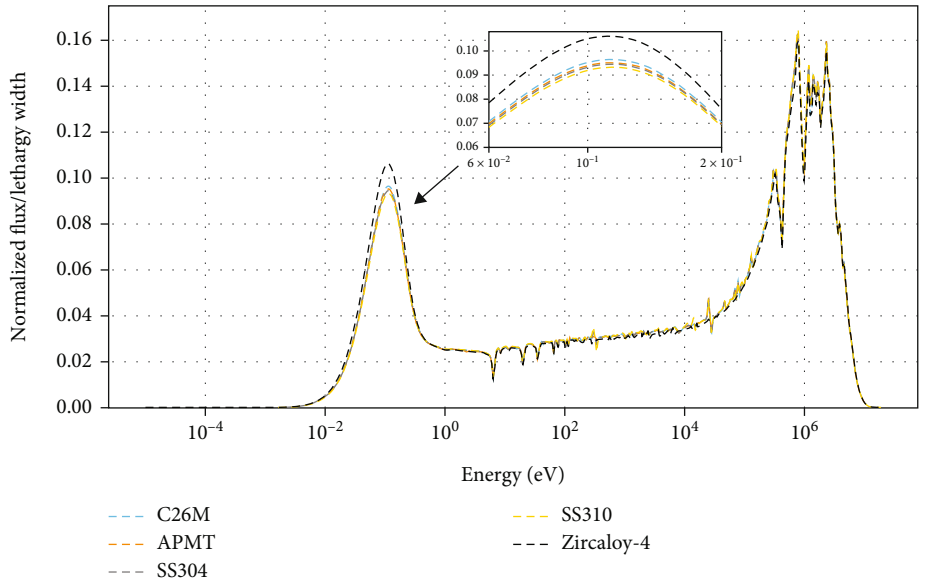

Figure 10: Spectrum of neutron flux for scenario 1.

predicting the multiplication factor for each case. In terms of deviation values, the ARO (all rods out) case demonstrated a lower value, whereas the A, B, C, D, SE, SD, and SC cases exhibited a higher value, indicating a difference of 14 and -235 pcm, respectively. It can be inferred that the model is reliable in predicting K_{eff} values, thereby providing a useful tool for evaluating the performance of nuclear reactors.

3.1.2. Control Rod Bank Worth. Using Equation (4) to determine the control rod bank worth, the criticality was

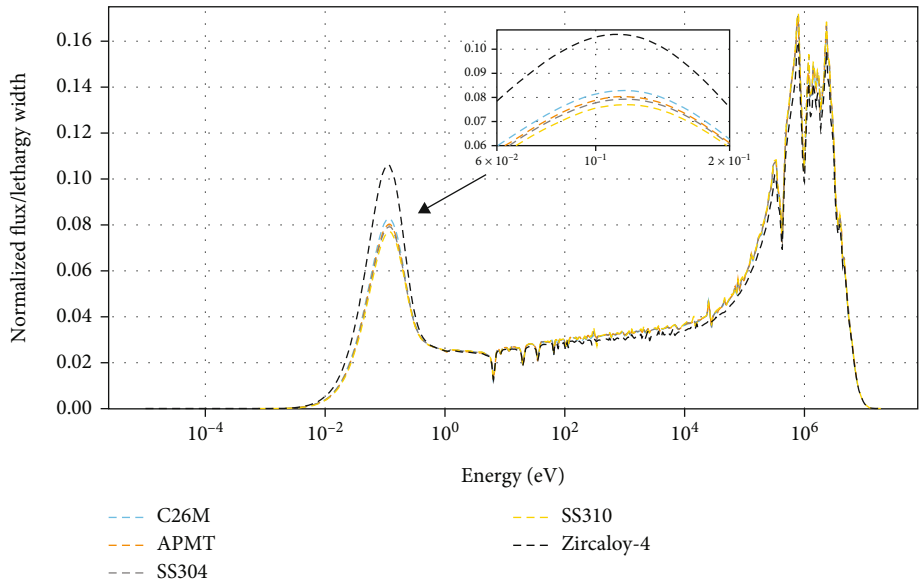

Figure 11: Spectrum of neutron flux for scenario 2.

compared between the configuration where all rods were withdrawn and the one where all control rod banks were inserted to calculate the control worth for bank D. Table 12 presents the resulting control worth for bank D, which showed a considerable agreement with the actual values, with only a slight difference of 15 pcm.

3.2. The Neutronic Penalty of Alternative Cladding Materials. The OpenMC code was used to simulate two cases, B-1-1 and B-1-2, which have the same parameters and dimensions except for changes in the cladding material type in B-1-1 and changes in both the cladding and grid spacer material in B-1-2. Table 13 shows the neutronic penalty resulting from the use of different materials due to the thermal neutron absorption cross-section. The lower and higher values of the neutronic penalty were observed for C26M and 310SS, respectively, with thermal neutron absorption cross-sections of 0.19 and 0.28 cm^{-1}. However, a significant drop in fuel reactivity was observed for various cladding materials, leading to a major reduction in the operational fuel-cycle length. Table 14 illustrates a slight increase in the neutronic penalty due to the change in grid spacer material, with values of -775, -910, -945, and -1056 pcm observed for C26M, APMT™, 304SS, and 310SS, respectively. As per reference [10], the predicted behaviour of penalty during depletion condition could potentially decrease due to neutron spectrum hardening. This hardening of the neutron spectrum results from fuel depletion, which leads to an overall increase in reactivity through an increased inventory of plutonium. Thus, the reactivity penalty that is noticed at the beginning of the cycle can undergo a significant reduction by the end of the cycle.

3.3. Parametric Study Matching Reactivity of Reference Zircaloy-4. To overcome the reactivity penalty associated with alternative cladding materials and match the performance of Zircaloy-4 cladding at the beginning of the cycle, modified fuel rod geometries or increased fuel enrichment

Table 17: The FTC and MTC of reactivity calculation for scenario 1.

Material	FTC (pcm/K)	MTC (pcm/K)
Zircaloy-4	-2.09	-28.25
C26M	-2.12	-42.59
APMT™	-2.13	-47.33
304SS	-2.24	-46.08
310SS	-2.23	-49.88

Table 18: The FTC and MTC of reactivity calculation for scenario 2.

Material	FTC (pcm/K)	MTC (pcm/K)
Zircaloy-4	-2.09	-28.25
C26M	-1.91	-38.26
APMT™	-2.02	-40.73
304SS	-2.03	-39.27
310SS	-2.06	-40.47

are necessary. Therefore, multiple iterations of simulations were conducted for alternative cladding materials to determine the appropriate enrichments and geometry for the fuel rods based on the three cases mentioned in the methodology section.

The case B-2 considered in this work is an increase in the U-235 enrichment level while keeping the thickness of the alternative cladding materials the same as the reference case. Table 15 illustrates the enrichment increase required to overcome the penalty observed at the beginning of the cycle. Raising the uranium enrichment level can cause various impacts on activities throughout the nuclear fuel cycle, beginning with nuclear fuel fabrication and extending through the storage and transportation of both fresh and irradiated fuel. Additionally, if the enrichment level exceeds

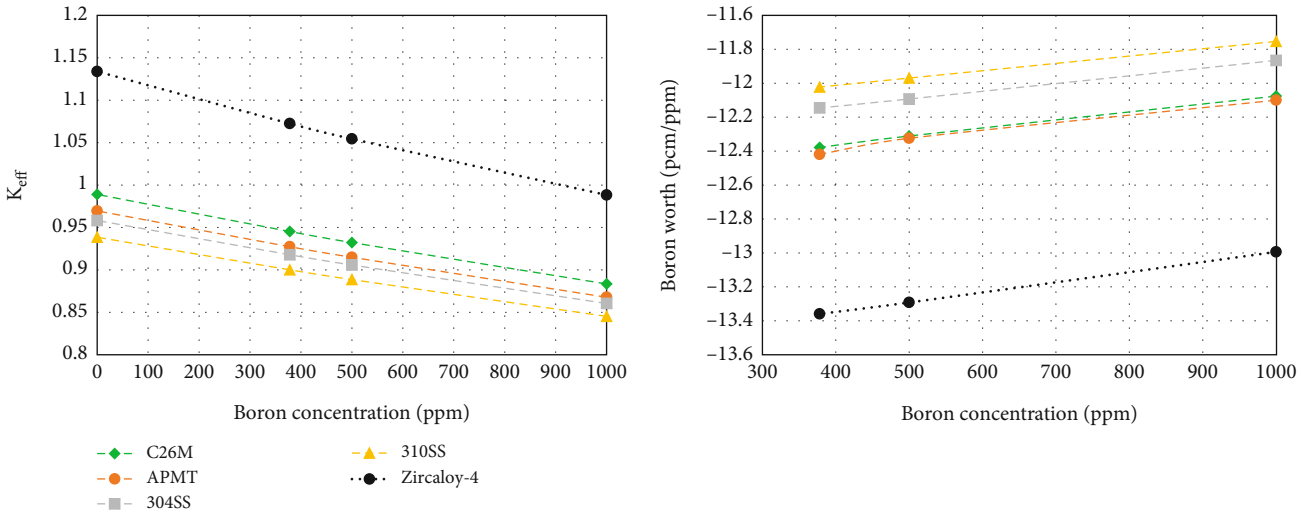

Figure 12: K_{eff} and boron worth coefficient as a function of boron concentration for scenario 1.

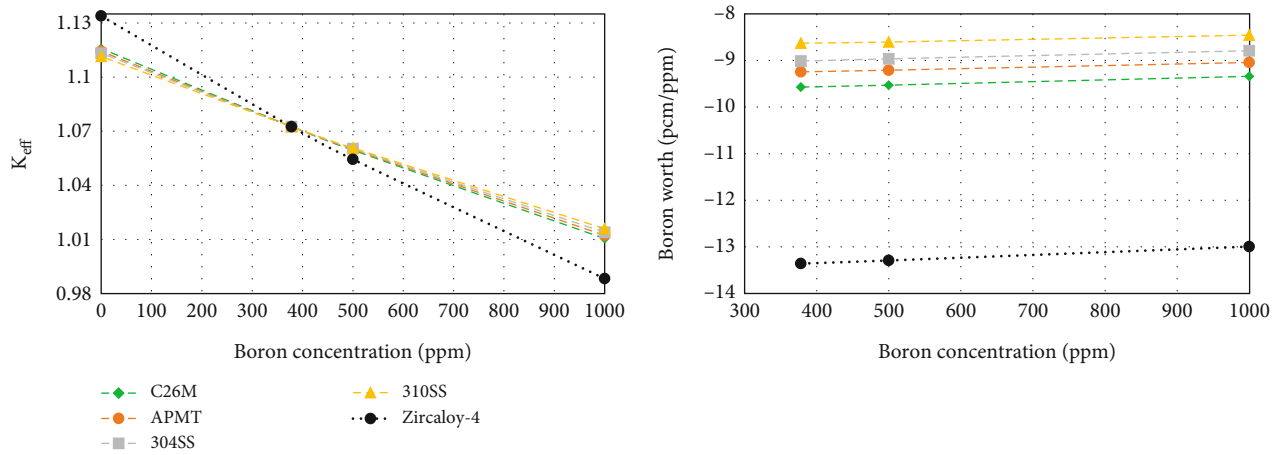

Figure 13: K_{eff} and boron worth coefficient as a function of boron concentration for scenario 2.

5.0%, all fuel cycle facilities will need to comply with a new licensing requirement. The reactivity required to compensate for the loss due to neutron absorption as a function of enrichment level for alternative cladding materials is shown in Figure 7. The enrichment levels range between 4.6% and 5.2% with respect to fuel type 3. Nevertheless, raising the enrichment level will affect fuel fabrication expenses. The required increase in enrichment level for C26M, APMT™, 304SS, and 310SS in each fuel type is 1.47%, 1.75%, 1.86%, and 2.15%, respectively, with respect to the reference case at the beginning of the cycle. The evaluation shows that there could be economic implications for the nuclear fuel cycle resulting from an enrichment increase.

Case B-3 is aimed at overcoming the reactivity penalty of alternative cladding materials while maintaining the fuel enrichments of fuel types 1, 2, and 3 at the same level as the reference case. This was achieved by reducing the thickness of the alternative cladding materials, which allowed for a proportional increase in fuel pellet diameter while preserving the same gap size and clad outer diameter. Figure 8 shows that the effective multiplication factor (K_{eff}) for various alternative cladding materials was plotted against cladding thickness. When the cladding thickness exceeds 350 μm, the effective multiplication factor for alternative cladding materials remains subcritical. However, as the cladding thickness decreases, K_{eff} increases. To overcome the observed penalty, the required cladding thickness decrease ranges from 30 to 1 μm for alternative cladding materials. However, excessively reducing cladding thickness could compromise fuel rod integrity in the reactor core. Therefore, reducing the thickness of alternative cladding materials may not be the most appropriate option at the beginning of the cycle.

Case B-4 was conducted to identify combinations of decreased cladding thickness and increased enrichment level of U-235 that could overcome the reactivity penalty. The thickness of alternative cladding materials was set to a reasonably conservative value of 350 μm which is consistent with the historical use of iron-based alloys as fuel cladding in LWRs [19]. Figure 9 shows the effective multiplication

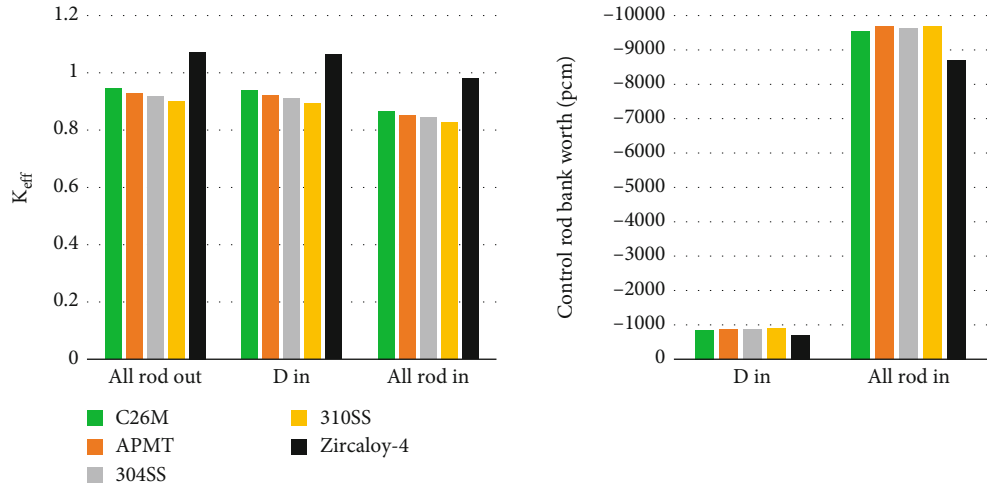

Figure 14: The K_{eff} and control rod worth for different configuration banks in scenario 1.

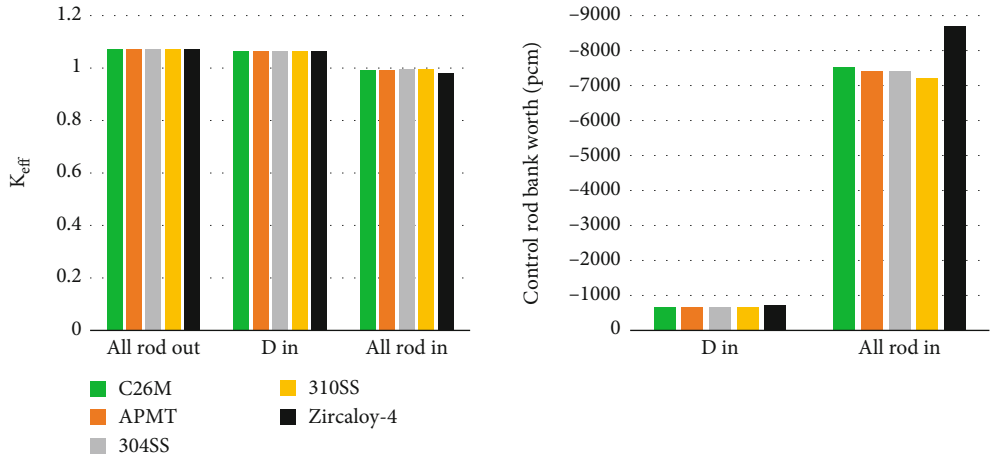

Figure 15: The K_{eff} and control rod worth for different configuration banks in scenario 2.

factor (K_{eff}) for various alternative cladding materials plotted as a function of the enrichment level in 350 μm of cladding thickness. Table 16 shows the enrichment increase required to overcome the penalty observed at 350 μm for C26M, APMT™, 304SS, and 310SS in each fuel type, which is 0.81%, 0.98%, 1.05%, and 1.23%, respectively, with respect to the reference case at the beginning of the cycle. Figures 7 and 9 illustrate that at an enrichment level of 4.40%, reducing the cladding thickness from 571.5 to 350 μm can contribute to an increase in the reactivity, with values of 4792, 5336, 5588, and 6099 pcm observed for C26M, APMT™, 304SS, and 310SS, respectively. During Cases 1-3, the lower and higher changes in enrichments and geometry for the fuel rods were C26M and 310SS, respectively. Additionally, APMT™ and 304SS showed almost identical responses. The results obtained indicate that the conditions of Case 3 are reasonably conservative and more economical compared to Cases 1 and 2.

3.4. Neutronic Analysis of Reactor Parameters. The effects of utilizing alternative cladding materials were evaluated on various factors, including the neutron spectrum, FTC, MTC, boron worth, control rod bank worth, power distribution, and thermal neutron flux distribution. The effects of using alternative cladding materials were examined based on two scenarios. Scenario 1 examined the impact of using alternative cladding materials while keeping the enrichment and geometry of the fuel rods as specified in the reference case. Meanwhile, scenario 2 evaluated the combined impact of using alternative cladding materials and modifications to the enrichments and geometry of the fuel rods obtained from case B-4. The reason for selecting the conditions of case B-4 is that they are reasonably conservative and more economical compared to those of case B-2 and case B-3.

3.4.1. Neutron Spectrum. The neutron flux spectra of both alternative cladding materials and the reference zircaloy cladding were analysed for scenarios 1 and 2, as depicted in Figures 10 and 11. The normalized flux spectra per unit lethargy were plotted with the energy range logarithmically divided into 500 energy groups spanning from 1×10^{-5} to 20×10^{6} eV.

	R	P	N	M	L	K	J	H	G	F	E	D	C	B	A
					0.584	0.733	0.850	0.818	0.863	0.754	0.610			Zircaloy-4 ref.	
					−0.282	−0.286	−0.294	−0.255	−0.291	−0.270	−0.264			C26M diff.	
1					−0.300	−0.298	−0.307	−0.256	−0.292	−0.280	−0.276			APMT diff.	
					−0.339	−0.344	−0.360	−0.319	−0.374	−0.363	−0.360			304SS diff.	
					−0.377	−0.375	−0.382	−0.327	−0.372	−0.356	−0.356			310SS diff.	
			0.642	0.920	0.932	0.824	0.988	0.873	1.009	0.849	0.963	0.951	0.669		
			−0.437	−0.508	−0.357	−0.152	−0.183	−0.081	−0.171	−0.128	−0.329	−0.474	−0.415		
2			−0.464	−0.540	−0.375	−0.150	−0.181	−0.074	−0.168	−0.126	−0.344	−0.505	−0.443		
			−0.539	−0.613	−0.417	−0.168	−0.210	−0.095	−0.220	−0.177	−0.452	−0.659	−0.576		
			−0.605	−0.694	−0.470	−0.175	−0.220	−0.088	−0.209	−0.154	−0.449	−0.668	−0.592		
		0.645	0.868	0.929	0.920	0.984	0.952	1.021	0.965	1.015	0.957	0.966	0.907	0.669	
		−0.427	−0.538	−0.370	−0.132	−0.020	0.084	0.089	0.096	0.008	−0.100	-0.333	−0.511	−0.417	
3		−0.463	−0.573	−0.389	−0.132	−0.013	0.101	0.108	0.112	0.015	−0.101	−0.355	−0.540	−0.435	
		−0.544	−0.668	−0.432	−0.133	−0.004	0.119	0.118	0.112	−0.007	−0.146	-0.463	−0.706	−0.567	
		−0.618	−0.756	−0.494	−0.149	0.005	0.142	0.148	0.154	0.030	−0.124	-0.466	−0.737	−0.594	
		0.920	0.933	1.253	1.075	1.027	1.188	1.082	1.208	1.061	1.112	1.295	0.970	0.956	
		−0.489	−0.356	−0.240	−0.009	0.174	0.265	0.298	0.292	0.208	0.029	−0.200	−0.330	−0.484	
4		−0.536	−0.376	−0.252	−0.007	0.193	0.289	0.323	0.316	0.225	0.031	−0.204	−0.346	−0.501	
		−0.628	−0.432	−0.263	0.017	0.234	0.338	0.363	0.342	0.239	0.006	−0.295	−0.460	−0.652	
		−0.713	−0.495	−0.302	0.020	0.265	0.387	0.418	0.404	0.294	0.047	−0.265	−0.468	−0.682	
	0.589	0.933	0.926	1.080	1.080	1.254	1.153	1.295	1.172	1.283	1.110	1.113	0.959	0.965	0.608
	−0.256	−0.330	−0.116	0.000	0.201	0.341	0.402	0.460	0.421	0.365	0.223	0.020	−0.104	−0.338	−0.271
5	−0.291	−0.365	−0.122	0.005	0.215	0.364	0.431	0.493	0.453	0.393	0.242	0.032	−0.096	−0.341	−0.277
	−0.340	−0.426	−0.131	0.026	0.261	0.430	0.494	0.555	0.502	0.428	0.255	0.005	−0.149	−0.445	−0.347
	−0.377	−0.477	−0.151	0.023	0.290	0.477	0.551	0.624	0.564	0.500	0.311	0.047	−0.129	−0.463	−0.369
	0.736	0.827	0.986	1.033	1.250	1.172	1.305	1.169	1.325	1.199	1.286	1.064	1.015	0.851	0.758
	−0.260	−0.127	−0.004	0.186	0.339	0.434	0.518	0.503	0.537	0.458	0.361	0.204	−0.002	−0.137	−0.276
6	−0.289	−0.145	−0.008	0.201	0.364	0.463	0.556	0.538	0.573	0.488	0.393	0.228	0.013	−0.129	−0.279
	−0.341	−0.163	0.005	0.247	0.435	0.535	0.636	0.604	0.639	0.538	0.429	0.242	−0.007	−0.171	−0.347
	−0.376	−0.180	0.004	0.267	0.478	0.588	0.702	0.669	0.714	0.606	0.496	0.292	0.025	−0.166	−0.367
	0.847	0.987	0.948	1.181	1.151	1.304	1.141	1.182	1.151	1.333	1.177	1.218	0.974	1.016	0.870
	−0.269	−0.156	0.098	0.270	0.404	0.515	0.512	0.525	0.524	0.536	0.416	0.282	0.092	−0.180	−0.289
7	−0.306	−0.185	0.095	0.284	0.428	0.552	0.548	0.564	0.560	0.579	0.455	0.316	0.119	−0.168	−0.285
	−0.353	−0.199	0.126	0.345	0.503	0.635	0.625	0.638	0.625	0.644	0.504	0.348	0.124	−0.212	−0.353
	−0.385	−0.221	0.142	0.378	0.550	0.698	0.682	0.698	0.689	0.716	0.567	0.406	0.155	−0.213	−0.371
	0.807	0.862	1.005	1.064	1.278	1.158	1.173	1.085	1.194	1.183	1.315	1.096	1.035	0.884	0.832
	−0.236	−0.066	0.096	0.293	0.448	0.495	0.521	0.515	0.539	0.514	0.463	0.301	0.090	−0.085	−0.265
8	−0.279	−0.092	0.087	0.302	0.471	0.525	0.554	0.547	0.569	0.551	0.503	0.332	0.111	−0.073	−0.262
	−0.302	−0.087	0.124	0.367	0.558	0.605	0.636	0.621	0.647	0.615	0.567	0.380	0.131	−0.082	−0.301
	−0.336	−0.094	0.140	0.403	0.611	0.660	0.693	0.677	0.709	0.677	0.630	0.420	0.154	−0.080	−0.327
	0.845	0.983	0.943	1.183	1.150	1.305	1.135	1.185	1.151	1.324	1.174	1.209	0.964	1.010	0.868
	−0.275	−0.162	0.099	0.281	0.404	0.522	0.514	0.533	0.525	0.532	0.412	0.271	0.085	−0.187	−0.303
9	−0.322	−0.199	0.088	0.285	0.425	0.550	0.542	0.559	0.553	0.567	0.446	0.301	0.101	−0.188	−0.313
	−0.340	−0.204	0.124	0.355	0.504	0.637	0.619	0.644	0.630	0.645	0.508	0.353	0.130	−0.194	−0.331
	−0.388	−0.230	0.136	0.384	0.545	0.695	0.673	0.700	0.684	0.704	0.557	0.391	0.144	−0.224	−0.386
	0.731	0.821	0.980	1.036	1.260	1.178	1.307	1.166	1.320	1.192	1.275	1.049	0.999	0.836	0.746
	−0.261	−0.128	0.002	0.197	0.351	0.445	0.522	0.504	0.531	0.446	0.340	0.178	−0.027	−0.159	−0.300
10	−0.305	−0.157	−0.011	0.203	0.367	0.465	0.548	0.528	0.557	0.475	0.372	0.200	−0.017	−0.162	−0.312
	−0.327	−0.160	0.004	0.250	0.436	0.537	0.633	0.608	0.644	0.546	0.440	0.246	0.006	−0.158	−0.326
	−0.372	−0.181	0.006	0.271	0.480	0.592	0.693	0.663	0.700	0.592	0.477	0.266	−0.004	−0.186	−0.388
	0.591	0.935	0.928	1.085	1.088	1.263	1.159	1.293	1.163	1.275	1.100	1.095	0.932	0.941	0.594
	−0.255	−0.320	−0.107	0.009	0.206	0.348	0.409	0.455	0.414	0.351	0.201	−0.014	−0.146	−0.380	−0.297
11	−0.292	−0.358	−0.117	0.012	0.222	0.369	0.432	0.475	0.428	0.366	0.213	−0.008	−0.145	−0.399	−0.313
	−0.325	−0.407	−0.127	0.022	0.263	0.430	0.499	0.555	0.505	0.441	0.270	0.025	−0.131	−0.421	−0.339
	−0.375	−0.479	−0.151	0.021	0.289	0.476	0.549	0.612	0.551	0.478	0.285	0.006	−0.168	−0.499	−0.395
		0.928	0.939	1.268	1.089	1.037	1.188	1.075	1.199	1.049	1.097	1.273	0.939	0.926	
		−0.469	−0.343	−0.227	0.002	0.185	0.272	0.295	0.276	0.192	0.000	−0.247	-0.386	−0.538	
12		−0.511	−0.361	−0.225	0.012	0.197	0.284	0.309	0.281	0.195	−0.013	−0.275	-0.416	−0.575	
		−0.593	−0.424	−0.270	0.016	0.231	0.336	0.363	0.348	0.251	0.027	−0.259	-0.435	−0.615	
		−0.706	−0.495	−0.308	0.017	0.259	0.377	0.405	0.386	0.267	0.007	−0.340	-0.532	−0.741	
		0.656	0.884	0.944	0.934	0.991	0.956	1.017	0.956	0.995	0.941	0.945	0.886	0.652	
		−0.419	−0.528	−0.357	−0.122	−0.013	0.088	0.087	0.088	−0.009	−0.116	−0.362	−0.545	−0.446	
13		−0.443	−0.548	−0.361	−0.113	−0.009	0.097	0.088	0.087	−0.021	−0.145	−0.409	−0.602	−0.488	
		−0.525	−0.657	−0.436	−0.138	−0.006	0.119	0.119	0.121	0.004	−0.126	−0.423	−0.658	−0.533	
		−0.624	−0.771	−0.500	−0.151	−0.004	0.139	0.140	0.137	−0.003	−0.161	−0.522	−0.795	−0.639	
			0.653	0.932	0.944	0.830	0.997	0.871	1.000	0.836	0.949	0.940	0.660		
			−0.423	−0.495	−0.343	−0.143	−0.176	−0.078	−0.172	−0.142	−0.347	−0.499	−0.432		
14			−0.445	−0.511	−0.355	−0.143	−0.185	−0.091	−0.198	−0.167	−0.399	−0.570	−0.484		
			−0.527	−0.619	−0.426	−0.168	−0.207	−0.089	−0.206	−0.167	−0.416	−0.608	−0.529		
			−0.621	−0.714	−0.480	−0.181	−0.226	−0.089	−0.226	−0.181	−0.487	−0.731	−0.638		
					0.595	0.736	0.849	0.820	0.859	0.741	0.600				
					−0.273	−0.280	−0.289	−0.253	−0.287	−0.280	−0.275				
15					−0.292	−0.300	−0.313	−0.281	−0.322	−0.314	−0.312				
					−0.344	−0.348	−0.355	−0.308	−0.345	−0.338	−0.337				
					−0.381	−0.385	−0.391	−0.335	−0.384	−0.380	−0.384				

Figure 16: Normalized radial power scenario 1.

Figure 10 illustrates the impact of using alternative cladding materials. The increased neutron-absorption cross-sections of the alternative cladding materials lead to a hardening of the thermal neutron flux spectrum. In contrast, Zircaloy-4 cladding material, with its lower absorption cross-section, leads to a higher inventory of thermal neutrons. Since thermal neutrons play a critical role in inducing fission, this reduced thermal neutron presence results in a

	R	P	N	M	L	K	J	H	G	F	E	D	C	B	A
1					0.584 −0.044 −0.045 −0.055 −0.060	0.733 −0.043 −0.040 −0.052 −0.055	0.850 −0.036 −0.025 −0.038 −0.042	0.818 −0.034 −0.023 −0.031 −0.037	0.863 −0.036 −0.012 −0.023 −0.036	0.754 −0.042 −0.017 −0.025 −0.044	0.610 −0.043 −0.022 −0.031 −0.044			Zircaloy-4 ref. C26M diff. APMT diff. 304SS diff. 310SS diff.	
2			0.642 −0.071 −0.063 −0.090 −0.098	0.920 −0.091 −0.081 −0.107 −0.122	0.932 −0.084 −0.080 −0.098 −0.109	0.824 −0.047 −0.041 −0.053 −0.053	0.988 −0.056 −0.043 −0.059 −0.064	0.873 −0.029 −0.018 −0.023 −0.026	1.009 −0.054 −0.033 −0.040 −0.053	0.849 −0.038 −0.016 −0.022 −0.039	0.963 −0.077 −0.050 −0.070 −0.090	0.951 −0.080 −0.055 −0.076 −0.097	0.669 −0.061 −0.054 −0.065 −0.082		
3		0.645 −0.068 −0.063 −0.084 −0.099	0.868 −0.130 −0.125 −0.159 −0.182	0.929 −0.116 −0.109 −0.133 −0.150	0.920 −0.053 −0.055 −0.060 −0.070	0.984 −0.032 −0.032 −0.031 −0.038	0.952 −0.001 0.003 0.012 0.011	1.021 −0.003 0.005 0.013 0.011	0.965 0.003 0.014 0.021 0.017	1.015 −0.022 −0.011 −0.005 −0.020	0.957 −0.039 −0.030 −0.029 −0.046	0.966 −0.096 −0.089 −0.102 −0.128	0.907 −0.110 −0.112 −0.131 −0.161	0.669 −0.048 −0.050 −0.066 −0.084	
4		0.920 −0.081 −0.081 −0.102 −0.117	0.933 −0.109 −0.106 −0.126 −0.149	1.253 −0.082 −0.071 −0.081 −0.106	1.075 −0.041 −0.044 −0.037 −0.051	1.027 0.019 0.015 0.037 0.032	1.188 0.044 0.043 0.072 0.075	1.082 0.063 0.064 0.088 0.093	1.208 0.066 0.068 0.091 0.094	1.061 0.040 0.039 0.060 0.057	1.112 −0.017 −0.022 −0.007 −0.020	1.295 −0.043 −0.049 −0.043 −0.066	0.970 −0.084 −0.089 −0.099 −0.127	0.956 −0.058 −0.062 −0.076 −0.100	
5	0.589 −0.032 −0.033 −0.048 −0.052	0.933 −0.071 −0.069 −0.084 −0.105	0.926 −0.045 −0.047 −0.046 −0.066	1.080 −0.038 −0.031 −0.024 −0.050	1.080 0.022 0.026 0.045 0.031	1.254 0.067 0.062 0.091 0.089	1.153 0.085 0.080 0.113 0.126	1.295 0.107 0.105 0.140 0.152	1.172 0.101 0.097 0.131 0.146	1.283 0.087 0.079 0.114 0.119	1.110 0.050 0.035 0.067 0.063	1.113 −0.007 −0.027 −0.005 −0.027	0.959 −0.023 −0.043 −0.027 −0.049	0.965 −0.053 −0.065 −0.063 −0.089	0.608 −0.027 −0.032 −0.032 −0.042
6	0.736 −0.028 −0.024 −0.042 −0.044	0.827 −0.030 −0.029 −0.039 −0.046	0.986 −0.021 −0.020 −0.021 −0.036	1.033 0.024 0.029 0.045 0.029	1.250 0.064 0.068 0.095 0.083	1.172 0.099 0.092 0.130 0.127	1.305 0.117 0.109 0.154 0.163	1.169 0.114 0.104 0.151 0.162	1.325 0.128 0.115 0.166 0.178	1.199 0.119 0.102 0.151 0.155	1.286 0.096 0.074 0.120 0.112	1.064 0.054 0.033 0.065 0.055	1.015 −0.003 −0.027 −0.003 −0.019	0.851 −0.017 −0.036 −0.020 −0.035	0.758 −0.017 −0.030 −0.021 −0.031
7	0.847 −0.023 −0.010 −0.035 −0.035	0.987 −0.041 −0.029 −0.051 −0.060	0.948 0.011 0.013 0.014 0.006	1.181 0.054 0.053 0.065 0.059	1.151 0.094 0.094 0.119 0.117	1.304 0.119 0.113 0.149 0.155	1.141 0.115 0.104 0.148 0.150	1.182 0.105 0.086 0.136 0.139	1.151 0.126 0.104 0.160 0.167	1.333 0.136 0.115 0.173 0.179	1.177 0.108 0.087 0.143 0.140	1.218 0.076 0.049 0.098 0.091	0.974 0.023 −0.001 0.031 0.023	1.016 −0.031 −0.055 −0.031 −0.046	0.870 −0.013 −0.030 −0.008 −0.015
8	0.807 −0.023 −0.012 −0.037 −0.038	0.862 −0.018 −0.011 −0.032 −0.033	1.005 0.006 0.012 −0.003 −0.014	1.064 0.064 0.061 0.068 0.067	1.278 0.106 0.104 0.124 0.123	1.158 0.113 0.107 0.139 0.146	1.173 0.107 0.093 0.134 0.132	1.085 0.112 0.092 0.139 0.142	1.194 0.116 0.097 0.148 0.152	1.183 0.127 0.112 0.167 0.169	1.315 0.116 0.094 0.156 0.156	1.096 0.078 0.054 0.102 0.101	1.035 0.016 −0.015 0.027 0.021	0.884 −0.012 −0.036 −0.007 −0.008	0.832 −0.015 −0.034 −0.013 −0.012
9	0.845 −0.020 −0.002 −0.046 −0.047	0.983 −0.045 −0.026 −0.073 −0.076	0.943 0.012 0.019 −0.008 −0.008	1.183 0.065 0.069 0.053 0.058	1.150 0.097 0.097 0.099 0.108	1.305 0.124 0.117 0.142 0.146	1.135 0.115 0.105 0.142 0.145	1.185 0.108 0.093 0.136 0.140	1.151 0.118 0.102 0.154 0.158	1.324 0.124 0.105 0.168 0.173	1.174 0.095 0.078 0.134 0.138	1.209 0.058 0.036 0.084 0.083	0.964 0.012 −0.014 0.023 0.026	1.010 −0.042 −0.070 −0.041 −0.044	0.868 −0.022 −0.042 −0.015 −0.017
10	0.731 −0.026 −0.008 −0.058 −0.055	0.821 −0.033 −0.017 −0.065 −0.062	0.980 −0.016 −0.005 −0.052 −0.051	1.036 0.039 0.044 0.019 0.024	1.260 0.079 0.087 0.069 0.078	1.178 0.108 0.108 0.115 0.125	1.307 0.116 0.112 0.141 0.147	1.166 0.111 0.105 0.142 0.151	1.320 0.116 0.105 0.153 0.163	1.192 0.099 0.085 0.136 0.146	1.275 0.063 0.046 0.100 0.105	1.049 0.019 0.002 0.042 0.048	0.999 −0.036 −0.057 −0.024 −0.024	0.836 −0.041 −0.065 −0.040 −0.037	0.746 −0.040 −0.057 −0.036 −0.035
11	0.591 −0.030 −0.015 −0.063 −0.060	0.935 −0.058 −0.040 −0.115 −0.112	0.928 −0.030 −0.019 −0.078 −0.070	1.085 −0.016 −0.011 −0.061 −0.053	1.088 0.040 0.045 0.017 0.032	1.263 0.076 0.082 0.070 0.087	1.159 0.095 0.092 0.103 0.117	1.293 0.097 0.093 0.122 0.133	1.163 0.084 0.082 0.117 0.128	1.275 0.063 0.055 0.095 0.106	1.100 0.019 0.013 0.045 0.055	1.095 −0.047 −0.065 −0.038 −0.030	0.932 −0.064 −0.082 −0.062 −0.057	0.941 −0.090 −0.113 −0.100 −0.098	0.594 −0.049 −0.061 −0.051 −0.050
12		0.928 −0.058 −0.040 −0.126 −0.115	0.939 −0.083 −0.070 −0.157 −0.147	1.268 −0.052 −0.030 −0.116 −0.103	1.089 −0.025 −0.013 −0.059 −0.047	1.037 0.027 0.032 0.014 0.027	1.188 0.048 0.053 0.045 0.059	1.075 0.054 0.060 0.068 0.082	1.199 0.042 0.042 0.064 0.078	1.049 0.015 0.017 0.036 0.051	1.097 −0.051 −0.049 −0.038 −0.024	1.273 −0.096 −0.098 −0.094 −0.074	0.939 −0.133 −0.142 −0.146 −0.141	0.926 −0.110 −0.117 −0.117 −0.113	
13		0.656 −0.050 −0.038 −0.103 −0.093	0.884 −0.102 −0.095 −0.187 −0.180	0.944 −0.088 −0.078 −0.160 −0.151	0.934 −0.037 −0.027 −0.081 −0.071	0.991 −0.023 −0.016 −0.055 −0.042	0.956 0.004 0.013 −0.011 0.007	1.017 −0.010 0.003 −0.016 0.002	0.956 −0.010 0.001 −0.003 0.012	0.995 −0.045 −0.030 −0.040 −0.023	0.941 −0.066 −0.055 −0.061 −0.043	0.945 -0.127 -0.119 -0.138 -0.124	0.886 −0.150 −0.144 −0.165 −0.158	0.652 −0.083 −0.083 −0.086 −0.087	
14			0.653 −0.049 −0.040 −0.106 −0.098	0.932 −0.064 −0.049 −0.135 −0.119	0.944 −0.062 −0.048 −0.120 −0.109	0.830 −0.034 −0.019 −0.069 −0.057	0.997 −0.048 −0.034 −0.089 −0.072	0.871 −0.029 −0.010 −0.051 −0.033	1.000 −0.060 −0.040 −0.082 −0.062	0.836 −0.053 −0.035 −0.060 −0.041	0.949 −0.094 −0.075 −0.102 −0.088	0.940 −0.100 −0.080 −0.103 −0.091	0.660 −0.080 −0.069 −0.088 −0.078		
15					0.595 −0.038 −0.021 −0.070 −0.062	0.736 −0.039 −0.020 −0.076 −0.063	0.849 −0.032 −0.008 −0.071 −0.058	0.820 −0.030 −0.006 −0.061 −0.047	0.859 −0.033 −0.011 −0.056 −0.039	0.741 −0.050 −0.027 −0.058 −0.047	0.600 −0.051 −0.033 −0.057 −0.047				

Figure 17: Normalized radial power scenario 2.

reduction in reactivity when spectral hardening occurs. Figure 11 demonstrates an increased spectral hardening effect compared to Figure 10 due to increased fuel enrichment while simultaneously reducing the cladding thickness.

3.4.2. Reactivity Coefficients. The investigation of the two reactivity coefficients (FTC and MTC) for alternative cladding materials was carried out under both scenarios 1 and 2. Meeting the safety standards of operational PWRs

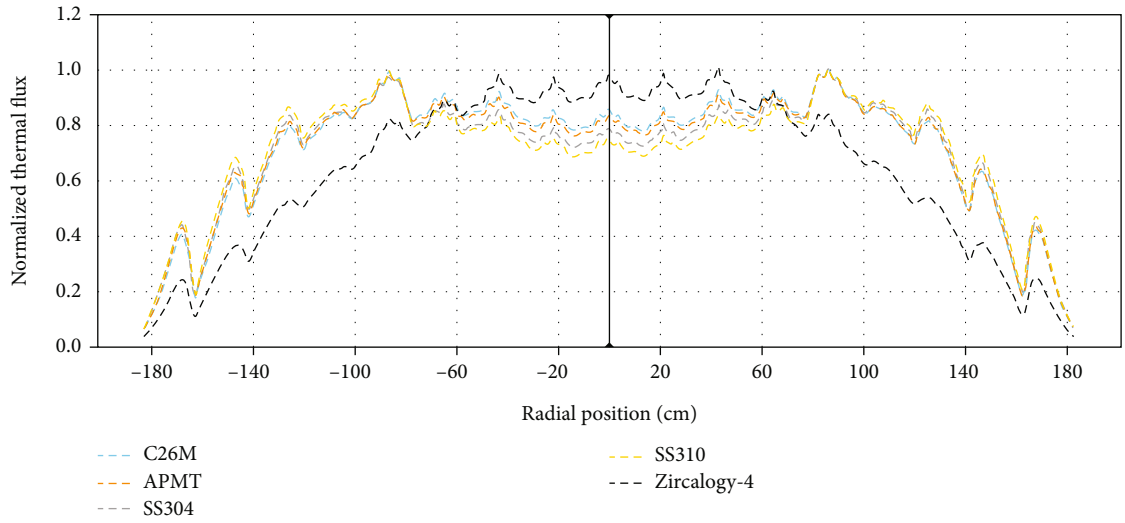

Figure 18: The radial thermal neutron flux distribution scenario 1.

requires maintaining negative values for all two coefficients in each cladding material.

Results from the study revealed that both reactivity coefficients yielded negative values for each cladding material in both scenarios 1 and 2, as outlined in Tables 17 and 18, respectively. The FTCs of alternative cladding materials closely resemble those of the Zircaloy-4 cladding. Nevertheless, the MTCs of alternative cladding materials show lower values relative to the Zircaloy-4 cladding with a deviation ranging from 14 to 21 pcm/K. This variance can be attributed to the higher absorption cross-sections of the cladding material and the resulting hardening of the neutron spectrum.

Furthermore, scenario 2 in Table 18 illustrates the effects of modifications to enrichments and geometry of fuel rods on the two reactivity coefficients. The FTCs of alternative cladding materials showed no discernible impact, whereas the MTCs observed decreased negative values compared to scenario 1. The differences amounted to -4.33, -6.6, -6.81, and -9.41 pcm/K for C26M, APMT™, 304SS, and 310SS, respectively.

3.4.3. Boron Worth. Dissolved boron, as a burnable absorber (BA), is used to suppress initial reactivity by providing a poisoning effect. As shown in Figures 12 and 13, for scenario 1 and 2, respectively, the BW calculation results are negative for all given boron concentrations, and the BW coefficient decreases with increasing boron concentration. In scenario 1, the alternative cladding materials exhibit a similar response for the BW coefficient, around -12 pcm/ppm, while the Zircaloy-4 cladding value is roughly -13 pcm/ppm. In scenario 2, the alternative cladding materials also exhibit a comparable BW coefficient response, around -9 pcm/ppm. However, it should be noted that the coefficient is lower in scenario 2, mainly due to modifications made to the enrichments and geometry in the fuel rods, but still yields a negative value.

3.4.4. Control Rod Worth. Control rod worth is crucial for ensuring the safety and control of reactors. It is calculated as the change in reactivity resulting from fully inserting the control rod bank(s) from the top position. Figures 14 and 15 depict the K_{eff} and control rod worth for different configuration banks in scenarios 1 and 2. In all configuration banks, the control rod contributes a negative value, and the control rod worth increases as the number of inserted banks increases.

In scenario 1, the alternative cladding materials exhibit similar responses to control rod worth. The values of control rod worth for C26M, APMT™, 304SS, and 310SS in D bank are -846, -863, -881, and -897 pcm, respectively, while the Zircaloy-4 cladding value is -712 pcm. It is important to note that the control rod worth of alternative cladding materials is higher than that of Zircaloy-4 due to the neutronic penalty associated with alternative cladding materials.

In scenario 2, the control rod worth of alternative cladding materials is smaller than that of the Zircaloy-4 cladding. This reduction can be attributed to the modified fuel rods and the fact that alternative cladding materials have a larger macroscopic thermal neutron absorption cross-section, which also has a similar effect to that of control rod. In other words, the spectrum hardening decreases the impact of control rod.

3.4.5. Radial Power Distribution. The radial power distribution was calculated for each assembly in both scenarios 1 and 2 at BOC, and the results are shown in Figures 16 and 17. The first row displays the normalized assembly power values for the Zircaloy-4 cladding, while the second to fifth rows indicate the differences in assembly power for the alternative cladding materials in comparison to the Zircaloy-4 cladding. It can be observed that scenario 1 shows differences in assembly power values compared to the Zircaloy-4 cladding due to the neutronic penalty associated with alternative cladding materials. On the other hand, scenario 2 demonstrates that the power values of alternative cladding materials are nearly identical to those of Zircaloy-4 cladding, with a maximum radial peak factor of 1.3 and a minimum power factor value of 0.6.

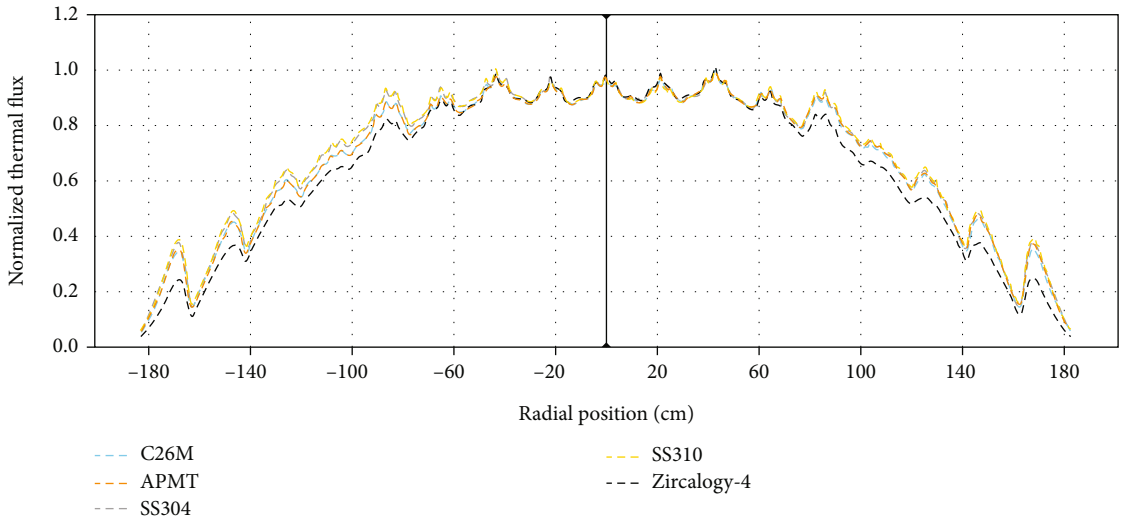

Figure 19: The radial thermal neutron flux distribution scenario 2.

3.4.6. Radial Thermal Neutron Flux Distribution. The radial thermal neutron flux was evaluated for scenarios 1 and 2 at BOC. The radial thermal neutron flux distributions are presented in Figures 18 and 19. In scenario 1, the Zircaloy-4 design had the highest thermal neutron flux at the center and gradually decreased towards the core boundary. Conversely, alternative cladding materials had a peak thermal flux at the middle of the radial length of the reactor core and decreased towards the core boundaries. This is because the high absorption cross-sections of the cladding material affect the hardening or softening of the neutron spectrum. In scenario 2, the thermal neutron flux distribution for alternative cladding materials was very similar to the reference at the center and then deviated from it, with the differences increasing towards the core boundaries.

4. Conclusions

In this study, neutronic analysis of accident-tolerant cladding materials in 3D Full Core BEAVRS PWR Benchmark was thoroughly investigated using OpenMC Code. The neutronic penalty associated with various alternative cladding materials was assessed in comparison to zirconium alloy in a 3D full PWR core at the beginning of the cycle (BOC). To conduct the calculations, the 3D BEAVRS core was simulated with cladding materials including C26M, APMT™, 304SS, 310SS, and Zircaloy-4.

The results revealed that the neutronic penalty varied for different alternative cladding materials in the reference case. Among the materials tested, C26M exhibited the lowest neutronic penalty, while 310SS demonstrated the highest. This disparity can be attributed to the high macroscopic thermal neutron absorption cross-section, which significantly affects the hardening of the neutron spectrum. Furthermore, when considering grid spacers, a slight increase in the neutronic penalty was observed. To address the reactivity penalty associated with the alternative cladding materials and achieve performance similar to that of Zircaloy-4, several options have been evaluated. Among these options, the third option (combinations of decreased cladding thickness and increased enrichment level of U-235) emerged as the most viable choice, being both reasonably conservative and economically feasible. A parametric analysis based on the third option demonstrated that C26M, APMT™, 304SS, and 310SS cladding could overcome the reactivity penalty of alternative materials and match the performance of Zircaloy-4 by reducing the cladding thickness to 350 μm and adjusting the enrichment level of U-235 to 0.81%, 0.98%, 1.05%, and 1.23%, respectively, for each material. Notably, C26M exhibited the lowest required enrichment level, while 310SS required the highest.

The fuel temperature coefficient (FTC), moderator temperature coefficient, boron worth, control rod bank worth, power distribution, and radial thermal neutron flux distribution were analysed for the alternative cladding materials, considering both the reference case and the modified fuel rods. The study investigated spectral hardening effects and observed that the utilization of alternative cladding materials with higher neutron-absorption cross-sections resulted in a hardening of the thermal neutron flux spectrum. This spectral hardening phenomenon is expected to notably amplify with increased levels of fuel enrichment and heavy metal loading. FTCs of alternative cladding materials were observed to closely resemble those of Zircaloy-4 cladding, while the MTCs showed slightly lower values from Zircaloy-4 cladding with a deviation value of -4.33 pcm/K for C26M. The boron worth coefficient showed no major impact, with all values remaining negative and similar to the Zircaloy-4 cladding. The reduced worth of the control rods in alternative cladding materials can be attributed to two factors. Firstly, the modification in the fuel rods itself contributes to this reduction. Secondly, alternative cladding materials have a larger macroscopic thermal neutron absorption cross-section, which has a similar effect to that of a control rod. In simpler terms, the influence of the control rod is diminished due to the spectrum hardening caused by these alternative cladding materials. It is crucial to ensure that the worth of the control rods meets the safety requirements when utilizing the alternative cladding materials.

Regarding the radial power distribution and radial thermal neutron flux distribution, discrepancies were observed between the alternative cladding materials and Zircaloy-4 cladding in the reference case. These variations stemmed from the neutronic penalty associated with the alternative materials. However, in the case of the modified fuel rods, the power values for the alternative cladding materials were nearly identical to those of Zircaloy-4 cladding. In contrast, the thermal neutron flux distribution for the alternative materials closely resembled that of Zircaloy-4 cladding at the center but deviated as it approached the core boundaries, with the differences becoming more pronounced.

The analysis results showed that C26M provided a significantly higher level of neutronic performance compared to APMT™, 304SS, and 310SS.

It is worth mentioning here that this study focuses only on the neutronic effects of alternative cladding materials in nuclear reactors at the BOC. Hence, in future research, it is imperative to evaluate the capabilities of these materials in terms of their mechanical and structural integrity under normal and severe accident conditions, with specific attention to the performance of the spacer grid, both with and without alternative cladding materials, conducting fuel depletion analysis to delve deeper into the potential of alternative cladding materials, especially in terms of fuel cycle length.

Data Availability

The data utilized to support the findings of this study can be obtained from the corresponding author upon request.

Conflicts of Interest

The authors declare that they have no conflict of interest.

Acknowledgments

The successful completion of this research was made possible by the invaluable support received from several institutions. Gratitude is extended to the Master's Degree in Nuclear Engineering program at the College of Engineering in King Saud University, King Abdulaziz City for Science and Technology (KACST), and King Abdullah City for Atomic and Renewable Energy (K.A.CARE). Special thanks are also due to the K.A.CARE Energy Research and Innovation Center at Riyadh, King Saud University, for their assistance in conducting the simulations on the computer, which significantly contributed to the research. Furthermore, this research received funding from the K.A.CARE Energy Research and Innovation Center at Riyadh, King Saud University, for which we are sincerely grateful. Their financial support played a crucial role in the successful execution of this research. This research received funding through a joint agreement between King Abdullah City for Atomic and Renewable Energy (K.A.CARE) and King Saud University, with grant number K.A.CAREKSU2022-3001.

References

[1] T. Murakami, "A historical review and analysis on the selection of nuclear reactor types and implications to development programs for advanced reactors; a Japanese study," *Energy Reports*, vol. 7, pp. 3428–3436, 2021.

[2] O. N. Pierron, D. Koss, A. T. Motta, and K. Chan, "The influence of hydride blisters on the fracture of Zircaloy-4," *Journal of Nuclear Materials*, vol. 322, no. 1, pp. 21–35, 2003.

[3] S. J. Zinkle and G. S. Was, "Materials challenges in nuclear energy," *Acta Materialia*, vol. 61, no. 3, pp. 735–758, 2013.

[4] Z. Duan, H. Yang, Y. Satoh et al., "Current status of materials development of nuclear fuel cladding tubes for light water reactors," *Nuclear Engineering and Design*, vol. 316, pp. 131–150, 2017.

[5] D. Diniasi, F. Golgovici, A. H. Marin, A. D. Negrea, M. Fulger, and I. Demetrescu, "Long-term corrosion testing of Zy-4 in a LiOH solution under high pressure and temperature conditions," *Materials*, vol. 14, no. 16, p. 4586, 2021.

[6] *The Fukushima Daiichi Accident, Non-Serial Publications*, IAEA, Vienna, 2015, https://www.iaea.org/publications/10962/the-fukushima-daiichi-accident.

[7] S. Gupta, "Experimental investigations relevant for hydrogen and fission product issues raised by the Fukushima accident," *Nuclear Engineering and Technology*, vol. 47, no. 1, pp. 11–25, 2015.

[8] "Development of light water reactor fuels with enhanced accident tolerance. Report to Congress April 2015".

[9] L. J. Ott, K. R. Robb, and D. Wang, "Preliminary assessment of accident-tolerant fuels on LWR performance during normal operation and under DB and BDB accident conditions," *Journal of Nuclear Materials*, vol. 448, no. 1-3, pp. 520–533, 2014.

[10] N. George, K. Terrani, and J. Powers, *Neutronic analysis of candidate accident-tolerant iron alloy cladding concepts*, ORNL/TM-2013/121, Oak Ridge National Laboratory, 2013.

[11] N. M. George, K. Terrani, J. Powers, A. Worrall, and I. Maldonado, "Neutronic analysis of candidate accident-tolerant cladding concepts in pressurized water reactors," *Annals of Nuclear Energy*, vol. 75, pp. 703–712, 2015.

[12] A. Naceur and G. Marleau, "Neutronic analysis for accident tolerant cladding candidates in CANDU-6 reactors," *Annals of Nuclear Energy*, vol. 113, pp. 147–161, 2018.

[13] N. T. Alhattawi, M. Alrwashdeh, S. A. Alameri, and M. M. Alaleeli, "Sensitivity neutronic analysis of accident tolerant fuel concepts in APR1400," *Journal of Nuclear Materials*, vol. 582, article 154487, 2023.

[14] X. B. Tran and N. Z. Cho, "A study of neutronics effects of the spacer grids in a typical PWR via Monte Carlo calculation," *Nuclear Engineering and Technology*, vol. 48, no. 1, pp. 33–42, 2016.

[15] A. Strasser, *An Evaluation of Stainless Steel Cladding for Use in Current Design LWRs*, Electric Power Research Institute, Palo Alto, Calif, 1982.

[16] K. A. Terrani, S. J. Zinkle, and L. L. Snead, "Advanced oxidation-resistant iron-based alloys for LWR fuel cladding," *Journal of Nuclear Materials*, vol. 448, no. 1-3, pp. 420–435, 2014.

[17] B. A. Pint, K. A. Terrani, M. P. Brady, T. Cheng, and J. R. Keiser, "High temperature oxidation of fuel cladding candidate materials in steam–hydrogen environments," *Journal of Nuclear Materials*, vol. 440, no. 1-3, pp. 420–427, 2013.

[18] A. S. Alomari, P. Joshi, and K. L. Murty, "High-Temperature Burst Creep Properties of Nuclear-Grade FeCrAl Fuel Cladding," in *Challenges in Mechanics of Time Dependent Materials, Mechanics of Biological Systems and Materials & Micro- and Nanomechanics, Volume 2*, Conference Proceedings of the Society for Experimental Mechanics Series, A. Amirkhizi, J. Notbohm, N. Karanjgaokar, and F. W. DelRio, Eds., Springer, Cham, 2022.

[19] N. George, *Assessment of reactivity equivalence for enhanced accident tolerant fuels in light water reactors, [Ph.D. thesis]*, University of Tennessee–Knoxville, Knoxville, TN, USA, 2015.

[20] S. B. Bell, K. A. Kane, C. P. Massey, L. A. Baldesberger, D. Lutz, and B. A. Pint, "Strength and rupture geometry of unirradiated C26M FeCrAl under LOCA burst testing conditions," *Journal of Nuclear Materials*, vol. 557, article 153242, 2021.

[21] N. Horelik, B. Herman, M. Ellis et al., *BEAVRS–Benchmark for evaluation and validation of reactor simulations*, Massachusetts Institute of Technology, Rev. 2.0.2. MIT Computational Reactor Physics Group, 2018.

[22] R. Rebak, L. Yin, T. Jurewicz, and A. Hoffman, "Acid dissolution behavior of ferritic FeCrAl tubes candidates for nuclear fuel cladding," *Corrosion*, vol. 77, no. 12, pp. 1321–1331, 2021.

[23] M. Suzuki and Y. Nauchi, *Analysis of BEAVRS revision 2.0 LWR whole core calculation using MVP with JENDL-4.0*, Korean Nuclear Society–KNS, Republic of Korea, 2017.

[24] "The OpenMC Monte Carlo Code," November 2022, https://docs.openmc.org/en/stable/.

[25] P. K. Romano, N. E. Horelik, B. R. Herman, A. G. Nelson, B. Forget, and K. Smith, "OpenMC: a state-of-the-art Monte Carlo code for research and development," *Annals of Nuclear Energy*, vol. 82, pp. 90–97, 2015.

[26] M. B. Chadwick, M. Herman, P. Obložinský et al., "ENDF/B-VII.1 nuclear data for science and technology: cross sections, covariances, fission product yields and decay data," *Nuclear Data Sheets*, vol. 112, no. 12, pp. 2887–2996, 2011.

[27] P. K. Romano, *Parallel Algorithms for Monte Carlo Particle Transport Simulation on Exascale Computing Architectures, [Ph.D. thesis]*, Massachusetts Institute of Technology, MA, USA, 2013.

[28] H. J. Park, S. J. Kim, H. Kwon, and J. Y. Cho, "BEAVRS benchmark analyses by DeCART stand-alone calculations and comparison with DeCART/MATRA multi-physics coupling calculations," *Nuclear Engineering and Technology*, vol. 52, no. 9, pp. 1896–1906, 2020.

[29] H. Lee, *Development of a New Monte Carlo Code for High-Fidelity Power Reactor Analysis, [Ph.D. thesis]*, Graduate School of UNIST, Ulsan, Republic of Korea, 2019.

[30] P. Darnowski and M. Pawluczyk, "Analysis of the BEAVRS PWR benchmark using SCALE and PARCS," *Nukleonika*, vol. 64, no. 3, pp. 87–96, 2019.

[31] M. S. Dwiddar, A. Badawi, H. A. Gabal, and I. A. El-Osery, "From VVER-1000 to VVER-1200: investigation of the effect of the changes in core," in *Conference: PHYTRA 3 – The Third International Conference on Physics and Technology of Reactors and Applications*, pp. 12–14, Tetouan, Morocco, May 2014.

[32] J. J. Powers, A. Worrall, K. R. Robb, N. M. George, and G. I. Maldonado, "ORNL analysis of operational and safety performance for candidate accident tolerant fuel and cladding concepts," in *Proceedings of a Technical Meeting 2016 (IAEA-TECDOC–1797). International Atomic Energy Agency (IAEA)*, Oak Ridge National Laboratories, USA, 2016https://www-pub.iaea.org/MTCD/publications/PDF/TE1797web.pdf.

[33] World Nuclear Association, "Uranium Enrichment," 2022, https://world-nuclear.org/information-library/nuclear-fuel-cycle/conversion-enrichment-and-fabrication/uranium-enrichment.aspx.

[34] Z. Benrhnia, O. Kabach, A. Chetaine et al., *Analysis of reactivity control coefficients and the stability of an AP1000 reactor assembly fueled with (Th-233 U) O2 using DRAGON code*, vol. 32, Annals of the University of Craiova, 2023.

[35] E. W. Lemmon, I. H. Bell, M. L. Huber, and M. O. McLinden, "Chapter thermophysical properties of fluid systems," in *NIST Chemistry WebBook, NIST Standard Reference Database Number 69*, P. J. Linstrom and W. G. Mallard, Eds., no. article 20899, 2022National Institute of Standards and Technology, Gaithersburg MD, 2022.